

Universal chaotic dynamics from Krylov space

Johanna Erdmenger,^a Shao-Kai Jian,^b and Zhuo-Yu Xian^{a,1}

^a*Institute for Theoretical Physics and Astrophysics and Würzburg-Dresden Cluster of Excellence ct.qmat, Julius-Maximilians-Universität Würzburg, D-97074 Würzburg, Germany*

^b*Department of Physics and Engineering Physics, Tulane University, New Orleans, Louisiana, 70118, USA*

E-mail: zhuo-yu.xian@physik.uni-wuerzburg.de

ABSTRACT: Krylov state complexity measures the spread of the wavefunction in the Krylov basis, a particular basis that is uniquely constructed using the Hamiltonian of a given physical system. Viewing each basis vector as one site, this basis naturally constitutes a one-dimensional chain, so that the state evolution can be mapped to a particle propagating on the chain, and its position is the Krylov state complexity. Based on this interpretation, we derive an Ehrenfest theorem for the Krylov complexity, which reveals its close relation to the spectrum. In particular, we find that the Krylov state complexity is directly driven by the properly normalized spectral form factor. This allows us to give an analytical expression for Krylov state complexity in random matrix theory. We also study the time evolution of the wavefunction in the Krylov basis. This provides the transition probability associated to the evolution of the initial state to the basis vector at a given site. For chaotic systems, including random matrix theories and the Sachdev-Ye-Kitaev model, we numerically observe a universal rise-slope-ramp-plateau behavior of the transition probability, with a long linear ramp. For the Gaussian unitary ensemble, we analytically explain this universal behavior for the sites located on the first half of the chain. The long linear ramp in the transition probability at each site leads to a peak in the Krylov complexity at late times. For non-chaotic systems, the transition probability shows a different behavior without the linear ramp. Our results clarify which features of the wave function time evolution in Krylov space characterize chaos.

¹Corresponding author.

²Authors' names are listed in alphabetical order.

Contents

1	Introduction	1
1.1	Outline and results	1
1.2	Chaos and Krylov space	2
1.3	Organization of the paper	6
2	Krylov state complexity	7
2.1	Krylov space	7
2.2	Krylov complexity of evolving states	9
2.3	Continuum limit	11
2.3.1	First-order formalism	11
2.3.2	Second-order formalism	13
2.4	Krylov complexity for the TFD state	14
3	Krylov complexity at early times	16
3.1	Lanczos coefficients in the large dimension limit	16
3.2	Krylov complexity from spectral form factor	19
3.2.1	Infinite temperature limit	21
3.2.2	Low temperature limit	22
3.3	Spectral complexity for Gaussian ensembles	22
4	Krylov complexity and chaos at late times	24
4.1	Numerical simulation	25
4.2	A first look at late times	26
4.3	Krylov complexity in the continuum limit	29
4.4	Confinement of polynomials	31
4.5	Chaos in transition probability	36
4.6	The peak of Krylov complexity	38
5	Non-chaotic spectrum	40
6	The SYK model	42
7	Conclusion and outlook	44
A	Imaginary time evolution	46

B Krylov approach in ensemble average	47
B.1 Krylov complexity in ensemble average	47
B.2 General linear ramp from Gaussian ensemble	49
B.3 Confinement in ensemble average	50
C Ramp down	53
D Constant Lanczos coefficients	53
D.1 Eigenstate	53
D.2 Large dimension limit	54
D.3 Finite dimension effects	55

1 Introduction

1.1 Outline and results

Krylov complexity measures the spread of a time-evolving state in a Hilbert space. For a maximally entangled state, this complexity only depends on the spectrum of the Hamiltonian and is independent of the choice of fundamental gates. We study the universal behavior of Krylov complexity for Hamiltonians describing chaotic systems. The Krylov approach consists of defining a particular Hilbert space basis, the Krylov basis. State evolution in this basis can be mapped to a particle moving on a one-dimensional chain. We exploit this map to equivalently describe state evolution in the Krylov basis in terms of forces acting on the particle. At early times, Krylov complexity displays a linear growth. Here we find that this linear growth is described by a generalized Ehrenfest theorem in Krylov space, providing an effective classical equation of motion for Krylov complexity. The linear growth of Krylov state complexity is not a characteristic of chaos, since it may also appear in non-chaotic systems. For late times, in chaotic systems Krylov complexity shows a characteristic peak and saturation structure, as numerically observed in Ref. [1]. By taking the continuum limit of the one-dimensional chain, we derive an analytical expression for the Krylov complexity at late times that confirms the observation of Ref. [1]. Moreover, we calculate the wave function in the Krylov basis. The mod of the amplitude squared of this wave function is referred to as transition probability. We find that it exhibits a universal rise-slope-ramp-plateau behavior with a long ramp. The ramp-plateau behavior is characteristic for chaos. Due to probability conservation, the characteristic long ramp that we find gives rise to the peak structure of the Krylov complexity. Moreover, we find that in non-chaotic systems, the long ramp of the transition probability disappears. This implies that in this case, the peak in the Krylov complexity is absent. Our results thus clarify which features of the wave function time evolution in Krylov space characterize chaos.

1.2 Chaos and Krylov space

To put our results into context, we begin with a brief review of quantum chaotic systems and the Krylov approach.

The time evolution of a quantum chaotic system are characterized by the statistics of the energy spectrum. In a quantum chaotic system, the energy levels are correlated and exhibit two salient phenomena: level repulsion and spectral rigidity [2–4]. Level repulsion refers to the fact that energy levels tend to avoid clustering. Spectral rigidity means that the number of levels within an energy interval of given size has small fluctuations. Both of these properties are due to the precise nature of correlations between level spacings in chaotic systems. More precisely, the level spacings in a chaotic system obey the Wigner-Dyson distribution [4]. The Wigner-Dyson distribution of the level spacing is straightforwardly obtained within random matrix theories (RMT) [3, 5]. The most studied RMT are the Gaussian ensemble of random matrices or the more general β -Gaussian ensemble [6], on which we will focus in this paper. Recently, the Sachdev-Ye-Kitaev (SYK) model [7, 8], a quantum mechanical model with all-to-all interactions (as opposed to nearest-neighbor interactions), was found to exhibit the level statistics of Gaussian RMT [9, 10]. Moreover, Jackiw-Teitelboim (JT) gravity, a two-dimensional dilaton gravity that shows similar features of the SYK model, is precisely consistent with a double-scaled random matrix integral [11].

The level statistics also determines the behavior of the spectral form factor (SFF) given by the square of the absolute value of the partition function with complex time argument [12, 13],

$$|Z(\beta + it)|^2 = \left| \text{Tr} e^{-(\beta+it)H} \right|^2 = \sum_{p,q=0}^{D-1} e^{-\beta(E_p+E_q)-it(E_p-E_q)}, \quad (1.1)$$

where E_p and D are the p -th eigenvalue and the dimension of the Hamiltonian H , respectively, and $\beta, t \in \mathbb{R}$. In a chaotic system, the SFF for the ensemble average usually shows three regions as a function of time: slope, ramp, and plateau [14–16], as shown in Fig. 1. Roughly speaking, these features arise from the width of the spectrum, spectral rigidity, and level repulsion, respectively. Since its time evolution reflects these properties, the SFF may be used to diagnose quantum chaos. The time at which there is a cross-over between the slope and ramp evolution is referred to as dip time. A chaotic system usually has an exponentially late dip time and an exponentially long and linear ramp region, controlled by the long-range spectral rigidity [2, 3, 14].

Chaotic evolution is a complicated process that requires a complexity measure for its quantitative analysis. Partially motivated by new relations between quantum computation and the time evolution of black holes [17–20], several concepts of complexity were proposed to measure how many computational steps are required

to reach a target state or operator from a reference state or operator. One of the motivations for the investigations in the present paper is to examine how complexity reflects late-time chaos, based on level repulsion and spectral rigidity.

Among the complexity measures in information theory, Nielsen defined the complexity of a unitary operator $U(t) = e^{-iHt}$ as the minimal distance to the identity in the unitary group [21–23]. The minimal distance on the group manifold is defined in terms of some cost function. The definition of the cost relies on the choice of few- or many-body terms based on the locality properties of the Hamiltonian H . A similar choice of fundamental operations appears in the notion of computational complexity, which measures the complexity of producing a target state $|\psi_T\rangle$ starting from a reference state $|\psi_R\rangle$ [24, 25]. Given a set of elementary quantum gates, the computational complexity is the minimum number of elementary gates necessary to achieve a unitary transformation U within a precision so that $|\psi_T\rangle = U|\psi_R\rangle$. Here, the ambiguity in defining complexity is related to the choice of gates. Both Nielsen’s complexity and computational complexity were investigated for free many-body systems and field theories [26–30], interacting systems [31–37], and for large qudit systems [38, 39].

When discussing the relation between late-time chaos and these notions of complexity, we note that level statistics does not provide the information about the locality properties of the Hamiltonian directly. Given a Hamiltonian from a Gaussian matrix ensemble, there is no natural way to define locality [15, 40], let alone few-body or many-body interaction terms. As we will describe below, Krylov complexity is unambiguously defined even in this case, and hence well-suited for matrix ensembles.

Notions of complexity were also proposed in the context of the AdS/CFT correspondence [41]. In particular, the volume or action of a wormhole connecting the two sides of an eternal black hole is conjectured to be related to the complexity of preparing the dual state in quantum field theory [18, 42–46]. The real-time evolution of holographic complexity exhibits a similar linear-to-plateau behavior as the computational complexity [47], where the growth rate is argued to be bounded by the energy [17]. Moreover, holographic complexity has a nonzero initial value that is proportional to the initial volume of the wormhole in the dual gravity theory. The eternal black hole corresponds to a thermofield double (TFD) state in the field theory [48]. So, the initial volume as well as the complexity are generated by imaginary time evolution in preparing the TFD state. So far, a precise holographic dual of complexity is still an open question, despite recent progress [45, 46, 49–54]. One of the remaining challenges is to precisely define complexity for interacting quantum field theories, in particular since their Hilbert space is infinite dimensional. One approach in this direction is to consider CFTs and to construct gates from conformal symmetry transformations [36, 37, 55–58]. This also allows to construct a gravity dual of the cost function [59].

With potential relations to holography in mind, the notion of Krylov complexity draws increasing attention [1, 60–66] since it is well-defined in any quantum theory. Krylov complexity has the advantage that its complexity measure is independent of the locality properties of the Hamiltonian. It does not rely on defining elementary gates or a given tolerance. This makes it very appealing in the context of holographic dualities. According to the Hilbert space on which Krylov complexity is defined, it describes the evolution of states [1] or operators [60], in both real time and imaginary time [67, 68].

In [1], a notion of Krylov *state* complexity is defined that realizes the appealing visualization of a wavefunction spreading over the Hilbert space in a basis-independent way. The authors of [1] refer to this Krylov state complexity as ‘spread complexity’. It measures how far the target state spreads in the Hilbert space \mathcal{H} . The target state $|\psi_\tau\rangle = e^{-\tau\mathcal{L}}|0\rangle$ starts from a reference state $|0\rangle$ at $\tau = 0$ and evolves under a Liouvillian operator \mathcal{L} constructed from the Hamiltonian H . Based on the Taylor series of \mathcal{L} , this evolution may be studied in *Krylov space* that is constructed by applying \mathcal{L} on $|0\rangle$ repeatedly. In the orthogonal and normalized basis of Krylov space, namely $\{|O_n\rangle\}$ with $|O_n\rangle = \psi_n(\mathcal{L})|0\rangle$ and $\psi_n(x)$ a polynomial of degree n , the Liouvillian \mathcal{L} becomes a tridiagonal matrix, whose components are called Lanczos coefficients [69, 70], denoted as $\{a_n, b_n\}$. In terms of the Krylov basis, the time evolution of a state $|\psi_\tau\rangle = e^{-\tau\mathcal{L}}|0\rangle$ can be effectively mapped to the propagation of a quantum particle along a one-dimensional chain, which is referred to as Krylov chain [60]. Krylov complexity is then defined as the location of the particle in the Krylov chain. This is equivalent to the expected number of times of applying \mathcal{L} on $|0\rangle$ required to generate $|\psi_\tau\rangle$.

Krylov *operator* complexity measures how far an operator in the Heisenberg picture spreads in the space of operators. By the Gelfand–Naimark–Segal (GNS) construction [71–73], the space of operators is isometric to a double-copy Hilbert space. More precisely, the reference state is defined as $|O\rangle = (O \otimes \mathbb{I})|0\rangle$, with O an arbitrary operator and \mathbb{I} the identity, acting on the single-copy Hilbert space, respectively, and $|0\rangle$ is a maximally entangled state in the double-copy Hilbert space. Moreover, one considers a Liouvillian $\mathcal{L} = H \otimes \mathbb{I} - \mathbb{I} \otimes H$, where H is the Hamiltonian acting on the single-copy Hilbert space. Since $\mathcal{L}|0\rangle = 0$, the application of \mathcal{L} on $|O\rangle$ is nothing but calculating the commutator, namely $\mathcal{L}|O\rangle = ([H, O] \otimes \mathbb{I})|0\rangle$. Then, the Krylov operator complexity $e^{-iHt}Oe^{iHt}$ is identified as the Krylov state complexity $e^{-it\mathcal{L}}|O\rangle$. Once the operator O has a nonzero commutator with the Hamiltonian, it will grow under the evolution with \mathcal{L} . Methods for studying the time evolution of Krylov complexity were recently obtained based on decomposing Liouvillian \mathcal{L} into annihilation and creation operators [65, 74, 75].

The exponential growth of Krylov operator complexity, and also the linear growth of Lanczos coefficients, allow to read out the Lyapunov exponent [60, 76] which characterizes the exponential operator size growth [77, 78] given by the out-of-time-ordered

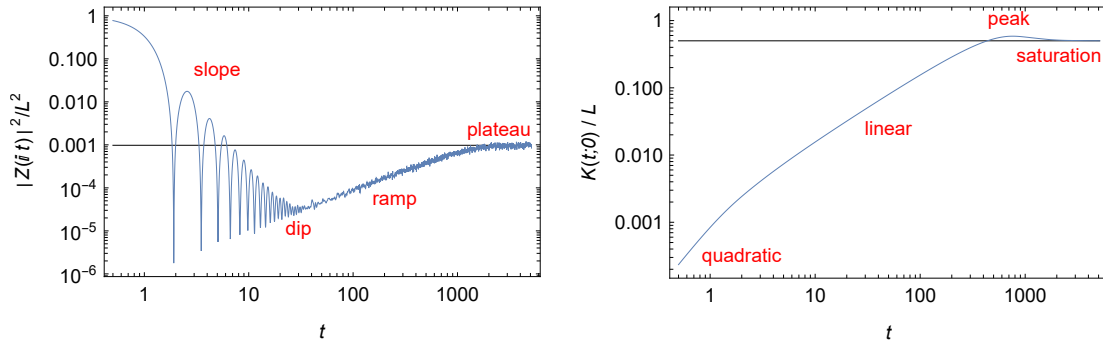


Figure 1. The SFF (left) and Krylov complexity of maximally entangled state (right) as functions of time for the Gaussian unitary ensemble with dimension $L = 1024$ and 128 realizations. The blue curves represent the numerical results and the black lines denote the values of $1/L$ (left) and $1/2$ (right).

correlator (OTOC) [79–82]. However, the maximally exponential growth of Krylov operator complexity at early times is also observed in integrable systems including free field theories. Exponential growth is therefore not necessarily related to chaos [64, 83]. Here, we hence also turn our attention to the relation between the late-time behavior of Krylov complexity and chaos [62, 84]. Moreover, it is argued in [85–88] that the descent in the Lanczos coefficients as well as the late-time behavior of the Krylov operator complexity given by the evolution with a chaotic Hamiltonian H is expected to be governed by the RMT. The relation between Krylov complexity and chaos has further been discussed for a number of models, including the SYK models [63, 89, 90], quantum field theories [91–95], many-body localization system [96], and open systems [97–100]. Krylov complexity has also been used for distinguishing topological phases [101, 102] and for investigating the quantum charging advantage of SYK-like quantum batteries [103].

To study late-time chaos from Krylov complexity, it appears to be more convenient to study Krylov state complexity directly. The Krylov complexity of maximally entangled state only depends on the spectrum of the Hamiltonian H . It is thus tied to the SFF and suitable to describe late-time chaos [1], in particular during the time range when the chaotic level spacing becomes manifest [62, 85]. In Fig. 1, we show the Krylov state complexity of the maximally entangled state corresponding to the SFF. It exhibits quadratic growth, linear growth, a peak, and saturation, whose transition time scales are close to those in the SFF. We refer to the time when it reaches its peak as “peak time.” We further refer to the quadratic growth and linear growth regions as early-time behavior and to the peak and saturation as late-time behavior. We will show that the early-time behavior is given by the double-time integral of the SFF via an Ehrenfest theorem and the late-time behavior is determined by the universal behavior of the probability given by the wave function in Krylov space.

1.3 Organization of the paper

In Sec. 2, we first review the construction of Krylov space and Krylov complexity. We introduce the continuum limit of the Krylov approach in a first-order and a second-order formalism, respectively. Moreover, we determine the Krylov complexity for obtaining the TFD state from a reference state given by a maximally entangled state. This Krylov complexity is entirely determined by the Hamiltonian spectrum.

In Sec. 3, we consider the Gaussian matrix ensemble and study the evolution of Krylov complexity at early times. We propose an Ehrenfest theorem for Krylov complexity, which linearly relates the second-order derivative of the Krylov complexity to the SFF, see (1.1). In particular, with the Lanczos coefficients given by Gaussian matrix ensemble, the linear growth of the Krylov complexity is determined by the slope of SFF, which is not necessarily related to chaos.

In Sec. 4, we study the evolution of a maximally entangled state in Krylov space at late times. For the Gaussian unitary ensemble (GUE), we numerically study the distribution and evolution of the *transition probability* $|\langle O_n | e^{-\tau \mathcal{L}} | 0 \rangle|^2$, namely the probability for reaching each state in the Krylov basis. We find that the transition probability universally exhibits a rise-slope-ramp-plateau behavior with an exponentially long ramp. Just like the SFF, the ramp-plateau behavior transition probability characterizes chaos. To analytically explain and estimate this behavior, we approximate the polynomial $\psi_n(\mathcal{L})$ and derive an expression for the rise-slope-ramp-plateau behavior. Moreover, we show that the above ramp-plateau behavior generally appears in any subspace observable in the Krylov space. Finally, we show that the existence of the long ramp in the transition probability is directly responsible for the peak in the Krylov complexity.

In Sec. 5, we study the transition probability and Krylov complexity for a non-chaotic spectrum, where the levels are uncorrelated. In contrast to the chaotic case, the transition probability here exhibits a rise-slope-plateau behavior without ramp. The absence of ramp in the transition probability is directly responsible for the absence of a peak in Krylov complexity. However, the linear growth of Krylov complexity persists.

In Sec. 6, we further study the transition probability and Krylov complexity in the SYK model. In the SYK₄ model, the transition probability exhibits a rise-slope-ramp-plateau behavior similar to the case of RMT. In the SYK₂ model, the transition probability exhibits a rise-slope-ramp-plateau behavior with a short ramp at small n and no ramp at large n .

We conclude in Sec. 7 with an outlook to future directions.

2 Krylov state complexity

In this section, we detail the general framework for Krylov space and Krylov complexity of a time-evolving state.

2.1 Krylov space

Given a Hilbert space \mathcal{H} , a reference state $|0\rangle \in \mathcal{H}$, and a Hermitian operator \mathcal{L} acting on \mathcal{H} called Liouvillian [60], we can construct the Krylov space as follows. First, we construct a sequence of normalized states $\{|A_j\rangle\}_{j=0}^{K-1}$ by subsequently applying \mathcal{L} to $|0\rangle$, namely $|A_j\rangle = \mu_{2j}^{-1/2} \mathcal{L}^j |0\rangle$, for $j = 0, 1, 2, \dots, K-1$, with $\mu_j = \langle 0 | \mathcal{L}^j | 0 \rangle$ the moments and K the minimal number such that $\mu_{2K} = 0$. In general, these states may not be independent of each other. Let L to be the index of the first state $|A_L\rangle$ becoming linearly dependent on the former states $\{|A_j\rangle\}_{j=0}^{L-1}$. Then its latter states $\{|A_j\rangle\}_{j=L}^{K-1}$ are also linearly dependent on these former states $\{|A_j\rangle\}_{j=0}^{L-1}$. So $\{|A_j\rangle\}_{j=0}^{K-1}$ only span a L -dimensional space \mathcal{K} , call Krylov space. Usually, we take the set of the former L states $\{|A_j\rangle\}_{j=0}^{L-1}$ as its basis.

In general, the states in the basis are not orthogonal to each other. We may apply the Gram-Schmidt orthogonalization to the sequence $\{|A_j\rangle\}_{j=0}^{L-1}$, which generate a sequence of orthogonal states given by

$$\{|O_n\rangle\}_{n=0}^{L-1}, \quad |O_n\rangle = \frac{1}{\sqrt{h_n}} p_n(\mathcal{L}) |0\rangle = \psi_n(\mathcal{L}) |0\rangle, \quad (2.1)$$

where $p_n(x)$ and $\psi_n(x)$ are respectively the monic and normalized orthogonal polynomial of degree n with a measure given by the spectrum of \mathcal{L} [104]. The norm h_n will be determined later. Define the projection on the Krylov space as $\pi_{\mathcal{K}} = \sum_{n=0}^{L-1} |O_n\rangle \langle O_n|$. Let $|E_p\rangle \in \mathcal{K}$ to be the eigenstate of $\mathcal{L}_{\mathcal{K}} = \pi_{\mathcal{K}} \mathcal{L} \pi_{\mathcal{K}}$, namely, $\pi_{\mathcal{K}} \mathcal{L} |E_p\rangle = E_p |E_p\rangle$ for $p = 0, 1, \dots, K-1$. The orthogonality relation and completeness relation are

$$\langle O_m | O_n \rangle = \langle 0 | \psi_m(\mathcal{L}) \psi_n(\mathcal{L}) | 0 \rangle = \int_E \psi_m(E) \psi_n(E) = \delta_{mn} \quad (2.2)$$

$$\sum_n \langle E_p | O_n \rangle \langle O_n | E_q \rangle = \langle E_p | 0 \rangle \langle 0 | E_q \rangle \sum_n \psi_n(E_p) \psi_n(E_q) = \delta_{pq} \quad (2.3)$$

where \sum_n is the shorthand of $\sum_{n=0}^{L-1}$ and the measure in \int_E on the spectrum $\{E_p\}$ of $\mathcal{L}_{\mathcal{K}}$ is defined as

$$\int_E f(E) \equiv \sum_p |\langle E_p | 0 \rangle|^2 f(E_p) = \int dE \rho(E) |\langle E | 0 \rangle|^2 f(E), \quad (2.4)$$

with the spectral density

$$\rho(\omega) = \sum_p \delta(\omega - E_p), \quad (2.5)$$

and a continuation of inner product $|\langle E_p|0\rangle|^2$. Formally, we can also write the completeness relation as $\sum_n \psi_n(E)\psi_n(E') = \delta(E - E')$, where the function $\delta(E - E')$ is defined as $\int_E \delta(E - E')f(E) = f(E')$.

The above Gram-Schmidt orthogonalization is realized by the following iterative algorithm [69, 70]

$$\begin{aligned} |O_0\rangle &= |0\rangle, \quad b_0 = 0, \\ b_n |O_n\rangle &= (\mathcal{L} - a_{n-1})|O_{n-1}\rangle - b_{n-1}|O_{n-2}\rangle, \quad 1 \leq n \leq L-1, \\ a_n &= \langle O_n|\mathcal{L}|O_n\rangle, \quad \langle O_n|O_n\rangle = 1. \end{aligned} \quad (2.6)$$

where $\{a_n, b_n\}$ are the Lanczos coefficients with the dimension of energy. By default, we choose $b_n \geq 0$. The Gram-Schmidt orthogonalization is equivalent to a tridiagonalization of the Liouvillian \mathcal{L} into a matrix \mathbf{L} ,

$$L_{mn} = \langle O_m|\mathcal{L}|O_n\rangle = \begin{pmatrix} a_0 & b_1 & 0 & \cdots & 0 \\ b_1 & a_1 & b_2 & \cdots & 0 \\ 0 & b_2 & a_2 & \cdots & 0 \\ \vdots & \vdots & \vdots & \ddots & b_{L-1} \\ 0 & 0 & 0 & b_{L-1} & a_{L-1} \end{pmatrix}. \quad (2.7)$$

The Lanczos coefficient can also be generated by the moments μ_j and vice versa. The Lanczos coefficients give the monic polynomials,

$$p_n(E) = \det(E - \mathbf{L}^{(n)}), \quad (2.8)$$

where $\mathbf{L}^{(n)}$ is the $n \times n$ sub-matrix $\{L_{pq}\}_{p,q=0}^{n-1}$. Obviously, the spectrum of \mathcal{L} are the roots of $p_L(E) = 0$. The norm h_n of the monic polynomial $p_n(E)$ is given by $b_n^2 = h_n/h_{n-1}$ and $h_0 = 1$. The polynomials satisfy the recurrence relation. For the normalized polynomials,

$$E\psi_n(E) = \sum_m L_{nm}\psi_m(E) = b_{n+1}\psi_{n+1}(E) + a_n\psi_n(E) + b_n\psi_{n-1}(E), \quad (2.9)$$

where $b_0 = b_L = 0$. From (2.2)(2.3), the n -th component of the eigenvector of \mathbf{L} for energy E_p is given by $v_n(E_p) = \langle 0|E_p\rangle \psi_n(E_p)$. Then the eigenstate of $\mathcal{L}_{\mathcal{K}}$ in \mathcal{K} can be written as $|E_p\rangle = \sum_n v_n(E_p)|O_n\rangle$.

Given a (non-normalized) state $|\psi\rangle \in \mathcal{K}$, we can expand it on the normalized orthogonal basis $\{|O_n\rangle\}_{n=0}^{L-1}$ as

$$|\psi\rangle = \sum_n |O_n\rangle \phi_n, \quad \phi_n = \langle O_n|\psi\rangle. \quad (2.10)$$

Then we can define the Krylov complexity of the state $|\psi\rangle$ as

$$K = J/P, \quad (2.11)$$

where

$$J = \sum_n n |\phi_n|^2, \quad P = \sum_n |\phi_n|^2. \quad (2.12)$$

2.2 Krylov complexity of evolving states

We consider the target state $|\psi_\tau\rangle$ generated by evolving the reference state $|0\rangle$ for time τ with \mathcal{L} , namely, [1, 66, 105]

$$|\psi_\tau\rangle = e^{-\tau\mathcal{L}}|0\rangle, \quad \tau = \beta + it, \quad \beta, t \in \mathbb{R}, \quad (2.13)$$

and $\langle\psi_\tau|\psi_\tau\rangle = S(2\beta)$, where $S(\tau) = \langle 0|e^{-\tau\mathcal{L}}|0\rangle$ is the *survival amplitude* for the state $|0\rangle$ to remain unchanged [1]. We have introduced the inverse temperature β and the real time t to study the complexity due to imaginary and real time evolution. Note that the imaginary time evolution in this paper is different from the finite temperature construction of the Krylov basis in [1], where the authors change the Krylov basis at finite temperature. Its expansion coefficient in (2.10) is

$$\phi_n(\tau) = \langle 0|\psi_n(\mathcal{L})e^{-\tau\mathcal{L}}|0\rangle = \int_E \psi_n(E)e^{-\tau E}. \quad (2.14)$$

In particular, the survival amplitude is $\phi_0(\tau) = \int_E e^{-\tau E} = S(\tau)$. If we regard $\phi_n(\tau)$ as a wave function at site n on the Krylov chain, it will obey the Schrödinger equation following the recurrence relation (2.9)

$$-\partial_\tau\phi_n(\tau) = b_{n+1}\phi_{n+1}(\tau) + a_n\phi_n(\tau) + b_n\phi_{n-1}(\tau), \quad (2.15)$$

with the initial condition $\phi_n(0) = \delta_{0n}$. The Krylov complexity (2.11) for the target state $|\psi_\tau\rangle$ is

$$K(t; \beta) = \frac{J(t; \beta)}{P(t; \beta)} \quad (2.16)$$

where

$$J(t; \beta) = \sum_n n |\phi_n(\beta + it)|^2, \quad (2.17)$$

$$P(t; \beta) = \sum_n |\phi_n(\beta + it)|^2 = S(2\beta). \quad (2.18)$$

Since $P(t; \beta)$ is the total probability, it is conserved under real time t evolution, which we indicate by defining $S(2\beta)$. In (2.18), the (non-normalized) *transition probability* is defined as

$$|\phi_n(\beta + it)|^2 = \int_{E, E'} e^{-\beta(E_1+E_2)-it(E_1-E_2)} \psi_n(E_1)\psi_n(E_2), \quad (2.19)$$

for the state $|0\rangle$ evolving to the Krylov state $|O_n\rangle$. In particular, the *survival probability* is given by the transition probability of $n = 0$, $|\phi_0(\tau)|^2 = |S(\tau)|^2$.

According to the Schrödinger equation (2.15), we have the imaginary time derivative

$$\partial_\beta P(0; \beta) = \sum_n [4b_{n+1}\phi_{n+1}(\beta)\phi_n(\beta) - 2a_n\phi_n(\beta)^2], \quad (2.20)$$

$$\partial_\beta J(0; \beta) = \sum_n [2(2n+1)b_{n+1}\phi_{n+1}(\beta)\phi_n(\beta) - 2na_n\phi_n(\beta)^2], \quad (2.21)$$

and the real time derivatives $\partial_t P(t; \beta) = 0$ and

$$\partial_t^2 J(t; \beta) = 2 \sum_{n=0}^{L-1} [(b_{n+1}^2 - b_n^2)\phi_n(\tau)\phi_n(\tau^*) - (a_{n+1} - a_n)b_{n+1}\phi_{n+1}(\tau)\phi_n(\tau^*)], \quad (2.22)$$

where $\tau = \beta + it$. (2.22) is just the expectation value of the commutator $\partial_t^2 \langle K \rangle = -\langle [[K, \mathcal{L}], \mathcal{L}] \rangle$. We refer to this equation as the *Ehrenfest theorem* of Krylov complexity, since it relates the second derivative of Krylov complexity to the expectation value of the gradient of the square of Lanczos coefficients. In this sense it provides a classical equation of motion for the Krylov complexity. This feature will become more clear in the continuum limit in App. (A). The version of Krylov operator complexity with $a_n = 0$ was derived in [104].

To calculate $K(t; \beta)$, we could start from $K(0; 0) = 0$, evolve it along imaginary time for β , get $K(0; \beta)$, evolve it along real time for t with the initial condition $\partial_t K(t; \beta)|_{t=0} = 0$, and finally get $K(t; \beta)$. Usually, we will integrate (2.22) over the real time and get the complexity difference $\Delta K(t; \beta) \equiv K(t; \beta) - K(0; \beta) = \int_0^t dt_2 \int_0^{t_2} dt_1 \partial_{t_1}^2 J(t_1; \beta) / S(2\beta)$. We discuss two limits of Krylov complexity below.

At the low temperature limit, we may use eigenstate with lowest two energies $E_{0,1}$ to approximate the wave function

$$\phi_n(\beta + it) \approx \psi_n(E_0)e^{-(\beta+it)E_0} |\langle E_0|0\rangle|^2 + \psi_n(E_1)e^{-(\beta+it)E_1} |\langle E_1|0\rangle|^2. \quad (2.23)$$

The Krylov complexity converges to a constant plus an oscillation with frequency $E_{10} = E_1 - E_0$, namely,

$$K_{\text{low}}(t; \beta) = |\langle E_0|0\rangle|^2 \sum_n n\psi_n(E_0)^2 + e^{-\beta E_{10}} 2 \cos(tE_{10}) |\langle E_1|0\rangle|^2 \sum_n n\psi_n(E_0)\psi_n(E_1). \quad (2.24)$$

Similarly to the SFF [14], the transition probability $|\phi_n|^2$ is determined by the energy levels in the long-time average, where oscillating phases average to zero and terms with $E_p = E_q$ survive, namely

$$(|\phi_n(\beta + it)|^2)_\infty \equiv \lim_{T \rightarrow \infty} \frac{1}{T} \int_0^T dt \sum_{pq} |\langle E_p|0\rangle|^2 |\langle E_q|0\rangle|^2 e^{-\beta(E_p+E_q)+it(E_p-E_q)} \psi_n(E_p)\psi_n(E_q) \quad (2.25)$$

$$= \sum_p |\langle E_p|0\rangle|^4 e^{-2\beta E_p} \psi_n(E_p)^2, \quad (2.26)$$

where we have assumed for simplicity that there is no degeneracy. We refer to the time when $|\phi_n|^2$ converges to this value as plateau time t_p . Then the long-time average of the complexity is given by

$$K_\infty(\beta) = \frac{1}{S(2\beta)} \sum_{pn} |\langle E_p | 0 \rangle|^4 e^{-2\beta E_p} n \psi_n(E_p)^2. \quad (2.27)$$

The late time average at $\beta = 0$ will be simplified if the reference state is taken to be a maximally entangled state in Sec. 2.4.

2.3 Continuum limit

It is difficult to solve the recurrence relation and Schrödinger equation with general Lanczos coefficients on the discrete Krylov chain. To simplify this problem, we consider the continuum limit $n \rightarrow x$, with x a continuous coordinate, and solve the corresponding differential equations.

2.3.1 First-order formalism

We may map the polynomials $\psi_n(E)$ and the wave function $\phi_n(\tau)$ to some continuous functions of n (as given below in (2.28) and (2.35)). Assuming that these functions depend smoothly on n , we may approximate their differences in n by their derivative w.r.t. n , and write the recurrence relation (2.9) and Schrödinger equation (2.15) as first-order differential equations [88, 104]. We refer to this approach as the first-order formalism of the continuum limit. Based on this simplifying approach, we may easily derive the Krylov complexity in the continuum limit. However, we will see that the assumption of smoothness is subtle and has to be clarified in a second-order formalism.

The authors of [88, 104] developed an approach to calculate the polynomial $\psi_n(E)$ and wave function $\phi_n(it)$ in the continuum limit as follows. The continuum limit is defined to take the form

$$x_n = \epsilon n, \quad \Psi(E, x_n) = i^n \psi_n(E), \quad \Phi(t, x_n) = i^n \phi_n(\beta + it), \quad b(x_n) = b_n, \quad a(x_n) = a_n, \quad (2.28)$$

which is valid when a_n , b_n , $i^n \psi_n(E)$, and $i^n \phi_n(\beta + it)$ are smooth functions of n . For real time t , the recurrence relation (2.9) and the Schrödinger equations (2.15) become

$$i(E - a)\Psi = \epsilon b' \Psi + 2\epsilon b \Psi' + O(\epsilon^2), \quad (2.29)$$

$$-(\partial_t + ia)\Phi = \epsilon b' \Phi + 2\epsilon b \Phi' + O(\epsilon^2), \quad (2.30)$$

where $b' = \partial_x b$, and equivalently for the other variables. The above two equations are related by the transformation (2.14) from energy E to time t . Due to the $\epsilon b' \Psi$

term in (2.29), the norm in (2.2) is not preserved by the evolution along x . Using the coordinate y with $dy = dx/(2\epsilon b(x))$ and with the new variable $\tilde{\Psi} = \sqrt{b}\Psi$ and $\tilde{\Phi} = \sqrt{b}\Phi$, these equations simplify to

$$(-iE + ia + \partial_y)\tilde{\Psi} = (\partial_t + ia + \partial_y)\tilde{\Phi} = 0. \quad (2.31)$$

Using the coordinate x , the solutions then become

$$\Psi(E, x) = \sqrt{\frac{b(0)}{b(x)}} \Psi(E, 0) \exp\left(i \int_0^x \frac{E - a(x')}{2\epsilon b(x')} dx'\right), \quad (2.32)$$

$$\Phi(t, x) = \frac{1}{\sqrt{b(x)}} f(t_-(t, x)) \exp\left(-i \int_0^x \frac{a(x')}{2\epsilon b(x')} dx'\right), \quad (2.33)$$

where the function $f(t_-)$ is determined by the initial condition and $t_-(t, x)$ labels the characteristic curves [104]

$$t_-(t, x) = t - \int^x \frac{dr}{2\epsilon b(r)}. \quad (2.34)$$

This shows that the wave function $\Phi(t, x)$ propagates forward with a local velocity $2\epsilon b(x)$, from $n = 0$ to $n = L$. Since the initial condition $\phi_n(0) = \delta_{0n}$ is highly discontinuous, the continuum limit is valid only when the wave function spreads out.

However, we notice that the discrete recurrence relation (2.9) and Schrödinger (2.15) enjoy the parity symmetry $n \rightarrow L - n$, but their continuum versions (2.29) and (2.30) break the parity $x \rightarrow -x$. As a result, the characteristic curves (2.38) have a preferred direction. The breaking of parity is due to our assumption how $i^n \psi_n(E)$ and $i^n \phi_n(it)$ depend on n in the continuum limit. If we consider an alternative continuum limit, namely

$$\Psi(E, x_n) = i^{-n} \psi_n(E), \quad \Phi(t, x_n) = i^{-n} \phi_n(it), \quad (2.35)$$

we find

$$-i(E - a)\Psi = \epsilon b'\Psi + 2\epsilon b\Psi' + O(\epsilon^2), \quad (2.36)$$

$$(\partial_t + ia)\Phi = \epsilon b'\Phi + 2\epsilon b\Phi' + O(\epsilon^2). \quad (2.37)$$

This result corresponds to the backward characteristic curves

$$t_+(t, x) = t + \int^x \frac{dr}{2\epsilon b(r)}. \quad (2.38)$$

This backward propagation will be important after the wave function is reflected by the edge at $n = L$. The forward propagation and backward propagation are unified by the second-order formalism presented in the next section.

Finally, we note that the polynomials $\psi_n(E)$ obtained from (2.32) have some artefacts. First, as a function of E , $\psi_n(E)$ is a Fourier mode of frequency $L(1 - \sqrt{1 - n/L})$ instead of a polynomial of degree n . Second, in general it does not obey the orthogonality and completeness relations (2.2)(2.3) and is not normalized to 1. Third, it usually takes a complex value. The first two artefacts are the results of continuum limit. Finally, since (2.29) does not preserve the normalization, we have to renormalize $\psi_n(E)$ for each n and E . The third artefact is solved by the second-order formalism as well.

2.3.2 Second-order formalism

We will adopt the following second-order formalism. Applying the recurrence relation (2.9) and Schrödinger equations (2.15) twice, we obtain

$$E^2\psi_n = \sum_{ml} L_{nm}L_{ml}\psi_l = c_{n+1}\psi_{n+2} + d_{n+1}\psi_{n+1} + e_n\psi_n + d_n\psi_{n-1} + c_{n-1}\psi_{n-2}, \quad (2.39)$$

$$-\partial_t^2\phi_n = \sum_{ml} L_{nm}L_{ml}\phi_l = c_{n+1}\phi_{n+2} + d_{n+1}\phi_{n+1} + e_n\phi_n + d_n\phi_{n-1} + c_{n-1}\phi_{n-2}, \quad (2.40)$$

where we dropped the arguments of $\psi_n(E)$ and $\phi_n(\tau)$ and the coefficients are

$$c_n = b_nb_{n+1}, \quad d_n = b_n(a_{n-1} + a_n), \quad e_n = b_n^2 + a_n^2 + b_{n+1}^2. \quad (2.41)$$

When $a_n = 0$ and then $d_n = 0$, the second-order formalism results (2.39) and (2.40) are factorized into even and odd parts, respectively. This happens in the case of even-parity spectrum $\{E_p\} = \{-E_p\}$ [104]. Consider even L for simplicity. The recurrences of even sector $\{\psi_0, \psi_2, \dots, \psi_{L-2}\}$ and odd sector $\{\psi_1, \psi_3, \dots, \psi_{L-1}\}$ are decoupled. The same applies to the evolution of wave function. It is therefore not appropriate in general to assume that the even sector smoothly connects to the odd sector. We therefore proceed as follows. We consider the continuum limit

$$x_n = \epsilon n, \quad \Psi(E, x_n) = i^n\psi_n(E), \quad \Phi(t, x_n) = i^n\phi_n(it), \quad c(x_n) = c_n, \quad g(x_n) = e_n - 2c_n, \quad (2.42)$$

where we assume that $\Psi(E, x_n)$ and $\Phi(t, x_n)$ are continuous at large L for even n and for odd n , respectively. The second-order formalism of (2.39) and (2.40) becomes, for either the even sector or the odd sector,

$$(-E^2 + g)\Psi = \epsilon^2(4c'\Psi' + c''\Psi + 4c\Psi'') + O(\epsilon^4), \quad (2.43)$$

$$(\partial_t^2 + g)\Phi = \epsilon^2(4c'\Phi' + c''\Phi + 4c\Phi'') + O(\epsilon^4). \quad (2.44)$$

Since these are real equations, we may obtain real solutions with real boundary conditions. Using the coordinate y with $dy = dx/(2\epsilon\sqrt{c(x)})$ and with the variables

$\tilde{\Psi} = c^{1/4}\Psi$, $\tilde{\Phi} = c^{1/4}\Phi$, these equations are simplified into two wave equations

$$(-E^2 - \partial_y^2 + V) \tilde{\Psi} = (\partial_t^2 - \partial_y^2 + V) \tilde{\Phi} = 0, \quad (2.45)$$

with potential $V = g - (\frac{1}{4}\partial_y \ln c)^2$. Thus, the characteristic curves are

$$t_{\pm}(t, x) = t \pm \int \frac{dx'}{2\epsilon\sqrt{c(x')}}. \quad (2.46)$$

They correspond to the forward and backward characteristic curves also given by the first-order formalism, (2.34) and (2.38). Since $\psi_0(E) = 1$ in the even sector and $\psi_1(E) = E/b_1$ in the odd sector, we impose the boundary conditions

$$\text{even } n : \quad \Psi(E, 0) = 1, \quad \Psi^{(0,1)}(E, 0) = 0, \quad (2.47)$$

$$\text{odd } n : \quad \Psi(E, 0) = 0, \quad \Psi^{(0,1)}(E, 0) = iE/b_1. \quad (2.48)$$

for simplicity of the solutions. The functions $\Psi(E, x)$ determined by solving the wave equations with the corresponding boundary conditions for the even sector and odd sector, respectively. A better approximation may be obtained by modifying the boundary conditions according to the values of $\psi_2(E)$ and $\psi_3(E)$.

2.4 Krylov complexity for the TFD state

The Krylov approach relies on the choice of the Liouvillian and reference state. In this subsection, to study the direct relation between chaos in the spectrum of a Hamiltonian H and Krylov state complexity, we will construct the Liouvillian from a Hamiltonian H and consider a maximally entangled state as the reference state. This is motivated by the construction of Ref. [1].

Consider a Hilbert space \mathcal{H} with dimension $D = \dim \mathcal{H}$, and a Hamiltonian H with eigenstates $|E_i\rangle_1$, $i = 0, 1, 2, \dots, D-1$, where the subscript “1” denotes the single Hilbert space. We consider a double-copy of the Hilbert space $\mathcal{H}_L \otimes \mathcal{H}_R$. Given a copy of energy basis $|E_i, E_j\rangle = |E_i\rangle_1 \otimes |E_j\rangle_1$, we can define a maximally entangled state in the double-copied Hilbert space

$$|0\rangle = \frac{1}{\sqrt{D}} U_L \otimes U_R \sum_{i=0}^{D-1} |E_i, E_i\rangle. \quad (2.49)$$

where $U_{L,R}$ is a unitary operator acting on $\mathcal{H}_{L,R}$. We will take $|0\rangle$ as the reference state. We consider the Liouvillian given by

$$\mathcal{L} = H \otimes \mathbb{I}, \quad (2.50)$$

where \mathbb{I} is the identity operator. Since the choice of unitary operators in (2.49) will not affect the moment $\langle 0 | \mathcal{L}^j | 0 \rangle$, we are free to choose $U_L = U_R = \mathbb{I}$. The Lanczos algorithm only depends on the spectrum of H .

The Krylov space \mathcal{K} is spanned by $\left\{ \mathcal{L}^n |0\rangle = (1/\sqrt{D}) \sum_i E_i^n |E_i, E_i\rangle \right\}$, which is a subspace of the space of equal-energy states $\mathcal{H}_{\text{eq}} = \{|E_i, E_i\rangle\}_{i=0}^{D-1}$. Their inner product can be written as the trace Tr in the single-copy Hilbert space,

$$\langle 0| f(\mathcal{L}) |0\rangle = \frac{1}{D} \sum_{i=0}^{D-1} f(E_i) = \frac{1}{D} \text{Tr} f(H), \quad (2.51)$$

Now the moment is $\mu_j = \text{Tr}[H^j]/D$, and especially, $b_1^2 = \langle 0| \mathcal{L}^2 |0\rangle = \text{Tr}[H^2]/D$. Notice that $\{E_i^n\}$ for $0 \leq i, n < D$ form a Vandermonde matrix, whose rank is the dimension of Krylov space $L = \dim \mathcal{K}$. L is reduced by the degree of degeneracy in the spectrum for the following reasons. Consider the decomposition $H_{\text{eq}} = \bigoplus_{p=0}^{l-1} \mathcal{H}_p$ where \mathcal{H}_p is a subspace with m_p -fold degeneracy $E_{p,0} = E_{p,1} = \dots = E_{p,m_p-1}$. For each \mathcal{H}_p , we may construct a basis where the first state is $|E_p\rangle = (1/\sqrt{m_p}) \sum_{k=0}^{m_p-1} |E_{p,k}, E_{p,k}\rangle$, which overlaps with the reference state as $\langle E_p|0\rangle = \sqrt{m_p/D}$, and the remaining $m_p - 1$ states are orthogonal to $|0\rangle$. Then the dimension of Krylov space is reduced by $m_p - 1$ for each \mathcal{H}_p . Since the Vandermonde matrix of the non-degenerate spectrum $\{E_p^n\}$ for $0 \leq p, n < l$ has full rank, L equals to the number of the non-degenerate energies, namely $L = l$. In this paper, we focus on the case that the spectrum is uniformly d -fold degenerate. So, the Krylov space of the maximally entangled state has dimension $L = D/d$ and overlap $|\langle E_p|0\rangle|^2 = 1/L$. Obviously, $\mathcal{L}_{\mathcal{K}}$ is diagonal on the the basis $|E_p\rangle$. Notice the difference between the the spectral density $\rho(E)$ of $\mathcal{L}_{\mathcal{K}}$ in (2.5) and the spectral density of H . The Krylov basis defined in (2.1) obeys the orthogonality and completeness relations (2.2)(2.3), with (2.4) equal to (2.51).

The target state

$$|\psi_\tau\rangle = e^{-\tau \mathcal{L}} |0\rangle = \frac{1}{\sqrt{D}} \sum_{i=0}^{D-1} e^{-\tau E_i} |E_i, E_i\rangle \quad (2.52)$$

with $\tau = \beta + it$ is a TFD state with inverse temperature 2β and evolved by the left side Hamiltonian for time t . Its coefficient on the Krylov basis, *i.e.* the wave function on the Krylov chain, is

$$\phi_n(\tau) = \frac{1}{D} \text{Tr}[\psi_n(H) e^{-\tau H}]. \quad (2.53)$$

Obviously, the survival probability is related to the SFF (1.1) as $|\phi_0(\tau)|^2 = (1/D^2) |Z(\tau)|^2$. With $S(2\beta) = Z(2\beta)/D$, the Krylov complexity is written as

$$K(t; \beta) = \frac{\sum_n n |\text{Tr}[\psi_n(H) e^{-(\beta+it)H}]|^2}{D \text{Tr}[e^{-2\beta H}]}. \quad (2.54)$$

Thus, the Krylov complexity for the TFD state only depends on the spectrum.

The Krylov space for the maximally entangled state has overlap $|\langle E_0|0\rangle|^2 = 1/L$. At $\beta = 0$, the long-time averages of the transition probability and of the Krylov complexity, given by (2.25) and (2.27), are simplified due to the orthogonality relation (2.2), as shown in [62, 87]:

$$(|\phi_n|^2)_\infty = \frac{1}{L}, \quad K_\infty = \frac{L-1}{2}. \quad (2.55)$$

These results are independent of whether chaotic behavior is present or not. They are essentially a consequence of taking the maximally entangled state as the reference state. However, we will show in Sec. 4.2 that the fluctuations of transition probability and Krylov complexity are indeed sensitive to the presence of chaotic behavior.

3 Krylov complexity at early times

Here, we will consider the Hamiltonian H drawn from the Gaussian orthogonal ensemble (GOE), the Gaussian unitary ensemble (GUE) and the Gaussian symplectic ensemble (GSE). They belong to the $\tilde{\beta}$ -Hermite (Gaussian) ensemble with Dyson index $\tilde{\beta} = 1, 2, 4$ respectively [6]. The measures of their random spectra are given by (B.9) in App. B. Due to the level repulsion in RMT, the spectra in both the GOE and GUE are non-degenerate, where $L = D$, and the spectrum in the GSE is doubly degenerate, where $L = D/2$. To simplify the notation, we are free to rescale the Hamiltonian so that the first Lanczos coefficient $b_1 = 1$. To recover the dimension, we can rescale the energies and times as $E_p \rightarrow E_p/\lambda$, $a_n \rightarrow a_n/\lambda$, $b_n \rightarrow b_n/\lambda$, and $\tau \rightarrow \tau\lambda$, where λ has the dimension of energy.

In Fig. 2, we display the Lanczos coefficients for the Krylov space of maximally entangled states for a realization of the GUE. When n increases, a_n fluctuates around 0 and b_n decreases from 1 to 0. Their expectation values in the large L limit are further discussed in Sec. 3.1. Their fluctuations become stronger when n increases.

In Fig. 3, we show the snapshots of the transition probability at some instants of real time t and imaginary time β in one realization of the GUE. Along the real time evolution, the profile consists of a shock wave, a long tail, and some residual noise following. The strength of the shock wave and the tail decrease along the time but the tail become longer. The shock wave becomes tiny when reaching the end of the Krylov chain. Along the imaginary time evolution, the wave function is localized to the ground state of the Schrödinger equation (2.15), which is similar to the fate of the wave function in the Krylov space of open systems [97–100].

In this section, we will develop an analytical approach for obtaining the evolution of Krylov complexity at early times.

3.1 Lanczos coefficients in the large dimension limit

For the Liouvillian drawn from the $\tilde{\beta}$ -Hermite ensemble and a fixed reference state $|0'\rangle$, the recent results of [66] show that the Lanczos coefficients obey the statistical

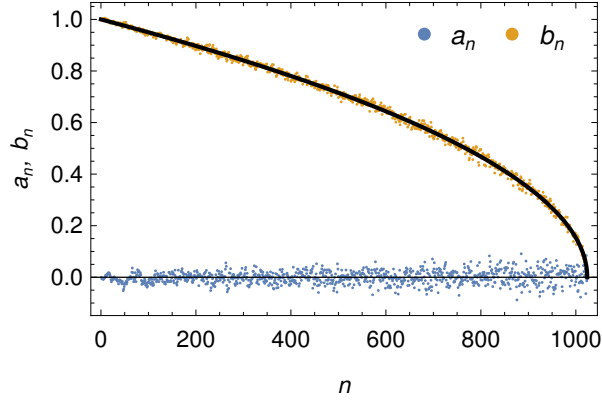


Figure 2. The Lanczos coefficients of a maximally entangled state evolving with the Liouvillian $\mathcal{L} = H \otimes \mathbb{I}$ where the H is taken from the GUE with dimension $D = 4096$. The black curve is a $\sqrt{1 - n/D}$.

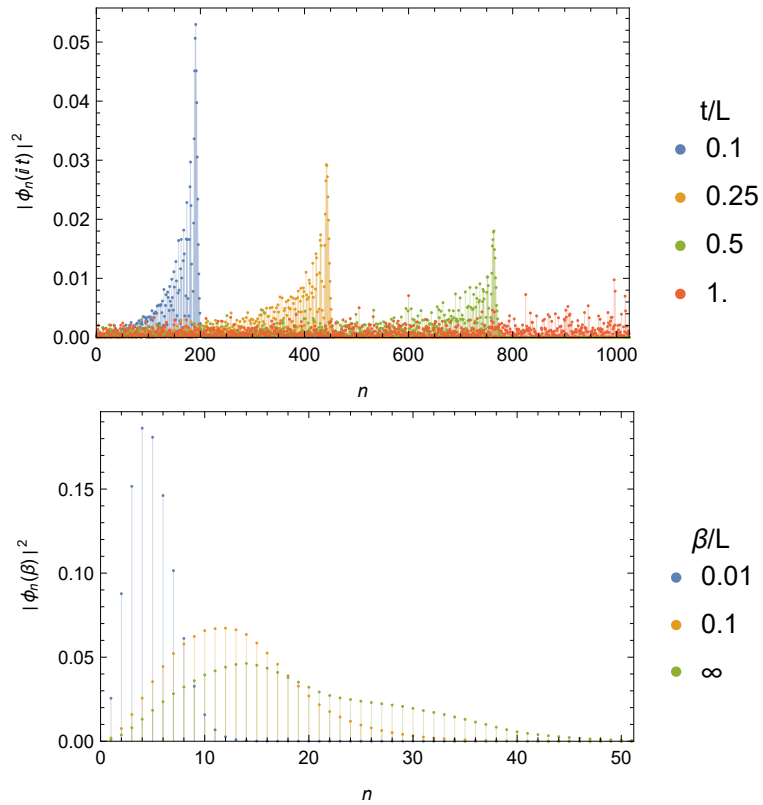


Figure 3. The snapshots of the transition probability $|\phi_n(it)|^2$ and $|\phi_n(\beta)|^2$ on the Krylov chain in one realization of the GUE with $L = 1024$.

distribution function

$$\rho(a_n) = \frac{1}{\sqrt{\tilde{\beta}L}} N(0, 2)(a_n), \quad \rho(b_n) = \frac{1}{\sqrt{\tilde{\beta}L}} \chi_{(L-n)\tilde{\beta}}(b_n), \quad (3.1)$$

where $N(r, s)$ is the Gaussian distribution with mean r and variance s , and $\chi_r(x)$ is the chi-distribution, given by $\chi_r(x) = 2^{-r/2} x^{r-1} e^{-x^2/2} / \Gamma(r/2)$.

The Lanczos coefficients have the expectation values and variance

$$\langle a_n \rangle = 0, \quad \Delta^2(a_n) = \frac{4}{\tilde{\beta}L}, \quad \langle b_n^2 \rangle = 1 - \frac{n}{L}, \quad \Delta^2(b_n^2) = \frac{2}{\tilde{\beta}L} \left(1 - \frac{n}{L}\right), \quad (3.2)$$

$$\langle b_n \rangle = \sqrt{\frac{2}{\tilde{\beta}L} \frac{\Gamma((L-n)\tilde{\beta}/2 + 1/2)}{\Gamma((L-n)\tilde{\beta}/2)}}, \quad \Delta^2(b_n) = 1 - \frac{n}{L} - \langle b_n \rangle^2, \quad (3.3)$$

where $\langle \dots \rangle$ denotes average over the $\tilde{\beta}$ -Hermite ensemble, and Δ^2 denotes the variance. In the large L limit, the variances are small compared to the average of b_n . Thus, we may take their expectation values in the large L limit,

$$a_n = 0, \quad b_n = \sqrt{1 - \frac{n}{L}}. \quad (3.4)$$

where the deviation from the convention $b_1^2 = 1$ is negligible for large L and we will maintain (3.4) for conciseness. In the continuum limit (2.28), the Lanczos coefficients become $a(x) = 0$, $b(x) = \sqrt{1 - x/(\epsilon L)}$ and the y coordinate is $y(x) = L \left(1 - \sqrt{1 - x/(L\epsilon)}\right)$. From the characteristic curves (2.46), the shock wave at time t will reach the site

$$n(t) = t \left(2 - \frac{t}{L}\right), \quad 0 < t \leq 2L. \quad (3.5)$$

Thus the shock wave reaches the last site at $t = L$. When $t > L$, the shock wave gets reflected and travels backward.

The authors of [66] gave an approximate way to related the density of state to the Lanczos coefficients in the large L limit. If we set $b_n = 0$ for relatively small number of n , *e.g.*, $n = ms$ for $m = 1, 2, \dots, r$ with integers $r, s \sim \sqrt{L}$ and $L = rs$, the density of state is approximately unaffected. This approach makes the tridiagonal matrix \mathbf{L} into a block diagonal matrix with r blocks of size $s \times s$. Furthermore, in the large L limit, the Lanczos coefficients change smoothly, *e.g.* (3.4). We can further approximate the a_n 's and b_n 's in the m -th block by their mean values \bar{a}_m, \bar{b}_m . From the case of constant Lanczos coefficients (D.7), the density of state in the m -th block is

$$\rho_m(E) = \frac{L}{s} \frac{\Theta(4\bar{b}_m^2 - (E - \bar{a}_m)^2)}{\pi \sqrt{4\bar{b}_m^2 - (E - \bar{a}_m)^2}}, \quad (3.6)$$

with normalization L/s . The total density of state is

$$\rho(E) = \sum_m \rho_m(E) \approx \frac{L}{\pi} \int_0^1 dx \frac{\Theta(4b(x)^2 - (E - a(x))^2)}{\sqrt{4b(x)^2 - (E - a(x))^2}} \quad (3.7)$$

where we have introduced $a_n = a(x)$, $b_n = b(x)$ in the continuum limit with $x = n/L$. Obviously, via (3.7), in the large L limit the Lanczos coefficients (3.4) give the semi-circle law

$$\rho_{\text{sc}}(E) = \frac{L}{2\pi} \sqrt{4 - E^2}. \quad (3.8)$$

With the above ingredients, in the next subsection we will find an analytical approximation to the Krylov complexity at early times.

3.2 Krylov complexity from spectral form factor

The Liouvillian \mathcal{L} in (2.50) is factorized and thus it is not a random Hamiltonian acting on the double-copy Hilbert space $\mathcal{H}_L \otimes \mathcal{H}_R$. The statistics of Lanczos coefficients (3.2) is not simply applicable. However, we find that if we take the limit (3.4) as the tridiagonalization of H and apply the algorithm (2.6) on the maximally entangled state $|0\rangle$ with the Liouvillian \mathcal{L} , we get the same Lanczos coefficients (3.4). In other words, the limit (3.4) is a fixed point of the algorithm on maximally entangled state (2.49). So, (3.4) may be taken as an approximation for the Lanczos coefficients of maximally entangled state in the large L limit, as shown in Fig. 2.

To proceed, we insert (3.4) into the Ehrenfest theorem (2.22) to get the following expression of the second derivative of Krylov complexity,

$$\partial_t^2 K(t; \beta) \approx 2 \frac{|S(\beta + it)|^2}{S(2\beta)} - \frac{2}{L} = \frac{2}{D} \frac{|Z(\beta + it)|^2}{Z(2\beta)} - \frac{2}{L} = \frac{2}{DZ(2\beta)} \sum_{p \neq q} e^{-\beta(E_p + E_q) - it(E_p - E_q)}, \quad (3.9)$$

where in the last expression, only the levels with different energies will contribute to the sum. This equation states that under the approximation for the Lanczos coefficient (3.4), the second derivative of Krylov is given by the SFF (1.1). In deriving this equation, we should note that the wave function also implicitly depends on the GUE Hamiltonian. Thus, we have actually neglected the statistical correlation between Lanczos coefficients and the wave function resulted from the GUE.

Surprisingly, if we take the double integral over the time on both sides of (3.9), we obtain exactly the *spectral complexity* defined in [106],

$$C(t; \beta) = \frac{1}{DZ(2\beta)} \sum_{p \neq q} \left[\frac{\sin(t(E_p - E_q)/2)}{(E_p - E_q)/2} \right]^2 e^{-\beta(E_p + E_q)}. \quad (3.10)$$

This implies that the Krylov state complexity and the spectral complexity are related by the Ehrenfest theorem in Krylov space. The authors of [88] also proposed an

equivalence between Krylov complexity and spectral complexity in the continuum limit. However, since we neglect the fluctuation of the Lanczos coefficients, we will see that the two complexities match each other through the linear growth region but deviate from each other at late times. We will distinguish the Krylov complexity K and its approximation from the Ehrenfest theorem, *i.e.* the spectral complexity C .

Notice that, beyond the plateau time, the SFF converges to the plateau value $|Z(\beta + it)|^2 \rightarrow dZ(2\beta)$ in ensemble average [14] with d -fold degenerate spectrum. Then (3.9) will vanish, which is a necessary condition for the saturation of spectral complexity C . However, it is not a sufficient condition, as (3.9) does not ensure that $\partial_t C(t; \beta)$ vanishes. In Ref. [106], the authors showed that for a chaotic system whose spectrum correlation is given by the GUE, the spectral complexity saturates at the late time. In other cases, we need to check this property case by case.

To approximate the Krylov complexity at early times, we will first consider the GUE and derive an analytical expression for the spectral complexity from the SFF at large L . We then discuss the cases of the GOE and GSE in a similar way at the end of this section. The spectral density $\langle \rho(E) \rangle$ at large L obeys the semicircle law (3.8), where the bracket is the matrix ensemble average. Its two-point correlation is given by the sine kernel [14–16]

$$\langle \rho(E_1) \rho(E_2) \rangle = \langle \rho(E) \rangle \delta(s) + \langle \rho(E_1) \rangle \langle \rho(E_2) \rangle \left[1 - \frac{\sin^2(\pi \langle \rho(E) \rangle s)}{(\pi \langle \rho(E) \rangle s)^2} \right], \quad (3.11)$$

where $s = E_1 - E_2$ and $E = (E_1 + E_2)/2$. The sine kernel shows the short-range correlation between the spectrum. By Fourier transformation, we obtain the SFF

$$\langle |Z(\beta + it)|^2 \rangle = |\langle Z(\beta + it) \rangle|^2 + \int dE e^{-2\beta E} \min \left\{ \frac{t}{2\pi}, \langle \rho(E) \rangle \right\}, \quad (3.12)$$

whose first (second) term is the disconnected (connected) part. From (3.8), the disconnected part is $|\langle Z(\beta + it) \rangle|^2 = \frac{L^2}{\beta^2 + t^2} |I_1(2\beta + 2it)|^2$, which contributes the slope of SFF. The connected part contributes to the ramp of SFF via the $t/2\pi$ in the integrand in the energy window satisfying $t < 2\pi \langle \rho(E) \rangle$ and contributes to the plateau when the energy window shrinks to zero.

We calculate the spectral complexity in the case of constant Lanczos coefficients in App. D. Here, we compare it to the spectral complexity in the GUE in the large L limit. At early times, the first term in (3.12) gives the same second derivative of complexity as in (D.11) given by the constant Lanczos coefficients. Integrating the second derivative along the time, we get the same linear growth rate of complexity as in (D.12) given by the constant Lanczos coefficients. It means that the linear growth in Krylov complexity is related to the disconnected part of the SFF. At late times, the second term in (3.12) starts to affect the behavior of spectral complexity in the GUE and leads to the deviation from the case of constant Lanczos coefficient.

Since we were not able to find an analytic formula for a general β [16], we will consider two limits $\beta = 0$ and $\beta \gg 1$ below.

3.2.1 Infinite temperature limit

We first consider the infinite temperature limit $\beta = 0$ so that the SFF and Krylov complexity are sensitive to the full spectrum. Evaluating the integral (3.12) with (3.8), we obtain the SFF [16, 107]

$$\langle |Z(it)|^2 \rangle = \text{Re} \left[\frac{t\sqrt{4L^2 - t^2} + 4L^2 \cos^{-1} \left(\frac{\sqrt{4L^2 - t^2}}{2L} \right)}{2\pi L} + \frac{L^2 J_1(2t)^2}{t^2} \right], \quad (3.13)$$

where J_n is the n -th Bessel function of the first kind. Inserting this into the Ehrenfest theorem (3.9) and taking the double-time integral with the initial condition $C^{(1,0)}(0;0) = C(0;0) = 0$, we obtain the spectral complexity

$$C(t;0) = L - 1 - \frac{16t}{3\pi} + {}_1F_2 \left(-\frac{1}{2}; 1, 2; -4t^2 \right) \quad (3.14)$$

$$+ \frac{L}{12\pi} \text{Re} \left[\frac{t}{L} \left(\frac{t^2}{L^2} + 26 \right) \sqrt{4 - \frac{t^2}{L^2}} - 24 \left(\frac{t^2}{L^2} + 1 \right) \sin^{-1} \left(\frac{\sqrt{4L^2 - t^2}}{2L} \right) \right],$$

which asymptotes to a constant at $t \rightarrow \infty$. More precisely, the spectral complexity has the asymptotic behavior

$$C(t;0) \rightarrow \begin{cases} t^2, & t \ll 1 \\ \frac{16}{3\pi}t, & 1 \ll t \ll L \\ L, & L \ll t \end{cases} \quad (3.15)$$

The comparison between our analytical expression and the numerical calculation for the Krylov complexity at $\beta = 0$ is shown in Fig. 1. They agree well before the peak time of the Krylov complexity. The linear growth $16t/3\pi$ is the result of the double-time integral of the slope of the SFF, which is totally determined by the spectral density and not the spectrum correlation. In App. D, we reproduce the same linear growth $16t/3\pi$ for constant Lanczos coefficients. We may therefore state that the linear growth is determined by the plateau of Lanczos coefficient and not related to chaos.

The saturation value of the spectral complexity $C(\infty;0) = L - 1$ is different from the saturation value of the Krylov complexity $K_\infty = (L - 1)/2$ in (2.55), as shown in Fig. 1. The saturation of the spectral complexity after the plateau time is due to the cancellation between the factor $\sin^2(\pi \langle \rho(E) \rangle x)$ in the sine kernel and the Fourier mode $\sin^2(tx/2)$ in (3.10) at either the imaginary infinity $x \rightarrow i\infty$ or $x \rightarrow -i\infty$. This saturation is related to chaos. Meanwhile, the saturation of the Krylov complexity for maximally entangled states is due to the discrete spectrum, which is not necessarily related to chaos.

3.2.2 Low temperature limit

In the low temperature limit $1 \ll \beta \ll L^{2/3}$, we may approximate the spectral density by the lower edge of the spectrum,

$$\rho(E) = \frac{L}{\pi} \sqrt{E}, \quad (3.16)$$

where we have shifted the energy as $E \rightarrow E - 2$ and considered $E \ll 1$, *i.e.* the “double scaled” limit [11, 14]. By evaluating (3.12), we obtain the SFF

$$\langle |Z(\beta + it)|^2 \rangle = \frac{L}{4\sqrt{2\pi}\beta^{3/2}} \operatorname{erf}\left(\frac{\sqrt{\beta}t}{\sqrt{2}L}\right) + \frac{L^2}{4\pi(\beta^2 + t^2)^{3/2}}, \quad (3.17)$$

with $\operatorname{erf}(z) = (2/\sqrt{\pi}) \int_0^z e^{-t^2} dt$ the error function. Using the Ehrenfest theorem (2.22) and taking the double-time integral, we obtain a change of complexity of the form

$$\Delta C(t; \beta) = \left(\frac{L}{\beta} + \frac{t^2}{L}\right) \operatorname{erf}\left(\frac{\sqrt{\beta}t}{\sqrt{2}L}\right) + \sqrt{\frac{2}{\pi\beta}} t \left(e^{-\frac{\beta t^2}{2L^2}} - 2\right) - \frac{t^2}{L} + 2\sqrt{\frac{2}{\pi\beta}} \left(\sqrt{\beta^2 + t^2} - \beta\right). \quad (3.18)$$

Asymptotically, we find

$$\Delta C(t; \beta) \rightarrow \begin{cases} \sqrt{\frac{2}{\pi\beta^3}} t^2, & t \ll \beta \\ 2\sqrt{\frac{2}{\pi\beta}} t, & \beta \ll t \ll L/\sqrt{\beta} \\ \frac{L}{\beta}, & L/\sqrt{\beta} \ll t \end{cases} \quad (3.19)$$

Similarly, the $\partial_t C(t; \beta) \rightarrow 0$ when $t \rightarrow \infty$ and then $C(t; \beta)$ saturates at late times. We compare the spectral complexity C to the numerical Krylov complexity in Fig. 4. They have the same quadratic-to-linear growth behavior, but asymptote to different saturation values at late times.

3.3 Spectral complexity for Gaussian ensembles

We may generalize the above calculation of the spectral complexity to GOE and GSE. Instead of integrating the SFF over time, we directly use the spectral complexity (3.10) and replace the two-point function (3.11) with [16]

$$\langle \rho(E_1) \rho(E_2) \rangle = \langle \rho(E) \rangle \delta(s) + \langle \rho(E_1) \rangle \langle \rho(E_2) \rangle - \frac{1}{2} \operatorname{Tr}(k(E_1, E_2) k(E_2, E_1)), \quad (3.20)$$

with

$$\text{GOE: } k(E_1, E_2) = \langle \rho(E) \rangle \begin{pmatrix} \hat{s}(X) & \mathbf{D}\hat{s}(X) \\ \mathbf{I}\hat{s}(X) - \epsilon(X) & \hat{s}(X) \end{pmatrix}, \quad (3.21)$$

$$\text{GUE: } k(E_1, E_2) = \langle \rho(E) \rangle \begin{pmatrix} \hat{s}(X) & 0 \\ 0 & \hat{s}(X) \end{pmatrix}, \quad (3.22)$$

$$\text{GSE: } k(E_1, E_2) = \langle \rho(E) \rangle \begin{pmatrix} \hat{s}(2X) & \mathbf{D}\hat{s}(2X) \\ \mathbf{I}\hat{s}(2X) & \hat{s}(2X) \end{pmatrix}, \quad (3.23)$$

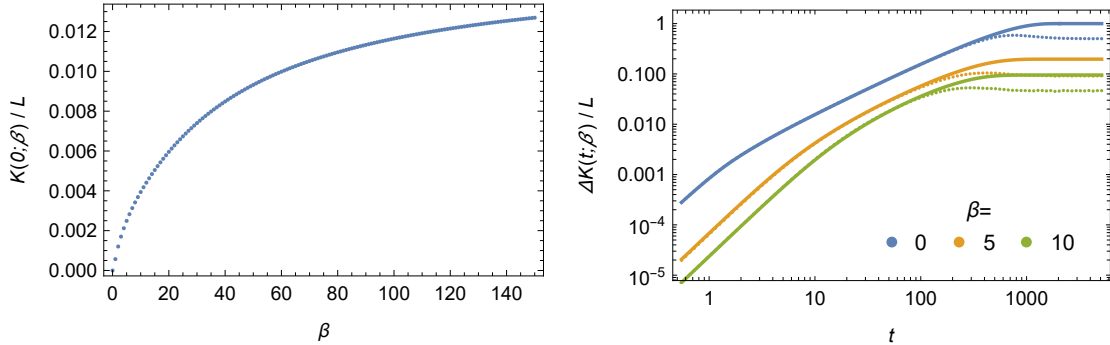


Figure 4. Krylov complexity as a function of inverse temperature (left) and time (right) for the GUE with $L = 1024$ and 64 realizations. The dots represent the numerical results and the solid curves represent analytical approximation from spectral complexity.

where

$$E = (E_1 + E_2)/2, \quad X = \pi \langle \rho(E) \rangle s, \quad s = E_1 - E_2, \quad (3.24)$$

$$\hat{s}(r) = \frac{\sin r}{r}, \quad \mathbf{D}\hat{s}(r) = \partial_r \hat{s}(r), \quad \mathbf{I}\hat{s}(r) = \int_0^r \hat{s}(t) dt, \quad \epsilon(r) = \frac{1}{2} \text{sgn}(r). \quad (3.25)$$

Similar to the case of JT gravity [106], the contact term in (3.20) will not contribute to the complexity. In all of the three Gaussian ensembles, the spectral complexity is always written as

$$\frac{2}{LZ(2\beta)} \int dE ds \langle \rho(E_1) \rangle \langle \rho(E_2) \rangle e^{-2\beta E} \left(\frac{1 - e^{its}}{s^2} \right) \left(1 - \hat{k}(\pi \langle \rho(E) \rangle s) \right), \quad (3.26)$$

with an ensemble-dependent kernel $\hat{k}(r)$, which behaves as $\hat{k}(r) \approx 1 + O(r)$ and $\hat{k}(r) \sim e^{i2dr} + e^{-i2dr}$ at $|r| \gg 1$, where $d = 1, 1, 2$ for the GOE, GUE, and GSE respectively. The integrand is therefore finite at $s = 0$. If $\hat{k}(r)$ is holomorphic, when $t > 2\pi d \langle \rho(E) \rangle$, we may close the contour of the s integral for those terms with the factor e^{its} . For this we use the arc at complex infinity in either the upper-half plane or the lower-half plane, such that the integral of those terms vanishes and the spectral complexity saturates. However, for the GOE, the sgn function in $\hat{k}(r)$ is not analytic. It will lead to a $\log t$ behavior in the spectral complexity even when $t > 2\pi \langle \rho(E) \rangle$.

To calculate the integral (3.26), we replace the E_1, E_2 with their mean value E . This affects the contribution of the disconnected part and is negligible at late times. For $\beta = 0$, the complexities in the GOE, GUE, and GSE grow as $16t/3\pi$ universally when $t \ll L$. They saturate to $L, (L/2) \log t$, and $2L/3$ respectively when $t \gg L$. In Fig. 5, we compare the spectral complexities derived from (3.26) with the numerical Krylov complexities. For each of the ensembles, both complexities have similar linear growth behavior at $t \ll L$, but have different limits for $t \gg L$. As we explained before, they saturate to different values since the saturation of spectral complexity is related to chaos while saturation of Krylov complexity is not.

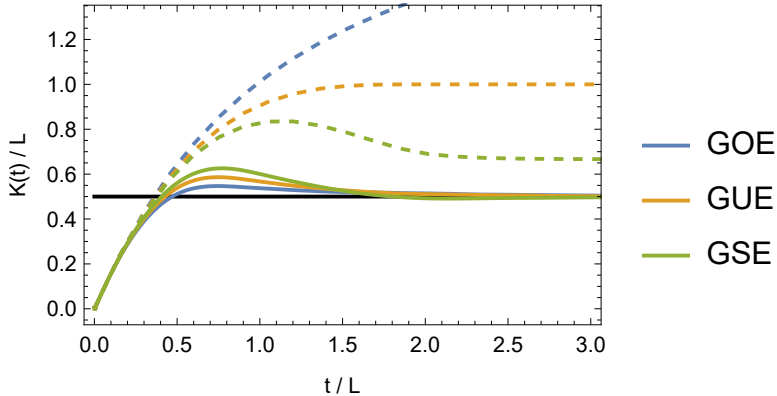


Figure 5. The Krylov complexities $K(t;0)$ (solid curves) of maximally entangled state and spectral complexities $C(t;0)$ (dashed curves) as functions of time t in the GOE, GUE, and GSE. The Krylov complexities are calculated numerically from the $\tilde{\beta}$ -ensemble with $L = 256$ and 128 realizations. The spectral complexities are derived from (3.26).

4 Krylov complexity and chaos at late times

Our calculations presented in the previous section demonstrate that the growth and saturation of Krylov state complexity are not significantly affected by the chaotic behavior of spectral statistics, such as spectral rigidity and level repulsion. Based on our analysis involving the Ehrenfest theorem, we find that the linear growth of Krylov complexity is mainly determined by the n dependence of the Lanczos coefficients b_n for small n , and the saturation is due to the discreteness of the spectrum. In fact, in Section 5, we demonstrate that the linear growth and saturation of the Krylov state complexity remain the same for non-chaotic spectra with uncorrelated levels.

The authors of Ref. [1] observed that the peak in Krylov complexity is sensitive to chaos. In this section, we focus on the late-time behavior of the transition probability $|\phi_n(\beta + it)|^2$ and Krylov complexity $K(t; \beta)$. In the transition probability, we discover a universal rise-slope-ramp-plateau behavior that includes a long ramp related to chaos. We find that the long ramp in the transition probability is responsible for the peak in the Krylov complexity.

Our analysis of the late-time behavior of the transition probability and the Krylov complexity in the GUE is organized as follows. In Sec. 4.1, we calculate the transition probability and Krylov complexity numerically and discuss their typical behavior. In Sec. 4.2, we examine their fluctuations and give a first look at the ramp and the saturation. In Sec. 4.3, we calculate the Krylov complexity in the continuum limit by ignoring the correlation between the spectral density and the polynomials of the Krylov basis. In Sec. 4.4, we study the significant effect of the correlation between the spectral density and these polynomials, which we call the confinement of polynomials. In Sec. 4.5, we revisit the transition probability by including the correlation between the spectral density and polynomials and discuss

further characteristics of chaos in the Krylov space. In Sec. 4.6, we examine the relationship between the ramp in the transition probability and the peak in the Krylov complexity.

4.1 Numerical simulation

The Krylov complexity (2.54) in the ensemble average may be written as

$$\langle K(t; \beta) \rangle = \frac{D}{\langle Z(2\beta) \rangle} \sum_n n \langle |\phi_n(\beta + it)|^2 \rangle. \quad (4.1)$$

To study the chaotic dynamic from the Krylov space, we further examine the transition probability $\langle |\phi_n(\beta + it)|^2 \rangle$ for the ensemble average of the GUE. This quantity records the square of the amplitude of the wave function in the n -th Krylov basis. In addition, we examine its disconnected part $|\langle \phi_n(\beta + it) \rangle|^2$ and connected part $\langle |\phi_n(\beta + it)|^2 \rangle_{\text{conn.}} = \langle |\phi_n(\beta + it)|^2 \rangle - |\langle \phi_n(\beta + it) \rangle|^2$. The former measures the square of the average amplitude of the wave function in the ensemble and the latter measures the correlation between the fluctuation of the wave function over the ensemble. Other observables in the Krylov space, such as the quantity in (2.11), can be split into their disconnected and connected parts in a similar manner. Our numerical simulation focuses on the case of $\beta = 0$ as the peak of the Krylov complexity is already significant at this value.

In Fig. 6, we show numerical snapshots of the probability wave $\langle |\phi_n(it)|^2 \rangle$ at different times in the ensemble average of the GUE with a large L and a huge number of realizations. We observe a shock wave with a long tail propagating forward and decaying during the evolution. Notably, it decays quickly when it reaches the end of the Krylov chain at $t \approx L$. The reflected wave is completely broken up. Once the shock wave pass by the Krylov chain, the global evolution of the probability wave is govern by diffusion. In particular, after $t \approx L$, the probability wave smoothly diffuses to a plateau value $1/L$, where the probability ramps up for $n \lesssim L/2$, and ramps down for $n \gtrsim L/2$.

In Fig. 7, we show the numerical time-evolution of the transition probability in the ensemble average $\langle |\phi_n(it)|^2 \rangle$, its disconnected part $|\langle \phi_n(it) \rangle|^2$, and its connected part $\langle |\phi_n(it)|^2 \rangle_{\text{conn.}}$ for various values of n . We observe a rise-slope-ramp-plateau behavior with a ramp-up for $n \lesssim L/2$ and a ramp-down for $n \gtrsim L/2$. This behavior has different features for different scales of n compared to L . Specifically:

$n \ll L$ The rise-slope is short and is mainly contributed by the disconnected part.

The ramp starts from a small step that depends on n , linearly increases, and then gradually slows down. The ramp is contributed by the connected part always, and gradually stops at a plateau time near $2L$.

$n \lesssim L/2$ The rise-slope becomes longer and is partially contributed by the connected part. The ramp starts from an obvious step below the plateau, linearly increases

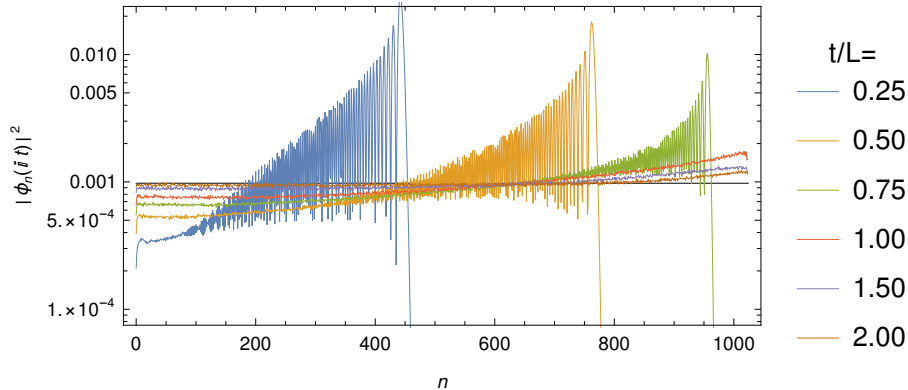


Figure 6. The snapshots of transition probability $\langle |\phi_n(it)|^2 \rangle$ for different t in chaotic system. We consider the GUE with $L = 1024$ and 4096 realizations. The black line denotes $1/L$.

with a smaller rate, and then gradually slows down. The plateau time is still near $2L$.

$L/2 \lesssim n < L$ The rise-slope is long and is mainly contributed by the connected part. The ramp starts from a step larger than the plateau, linearly decreases, and then gradually slows down. The plateau time is obviously greater than $2L$.

In Fig. 8, we show the numerical time-evolution of the Krylov complexity in the ensemble average $\langle K(t; 0) \rangle$, as well as its disconnected part $\sum_n n \langle |\phi_n(it)|^2 \rangle$, and its connected part $\sum_n n \langle |\phi_n(it)|^2 \rangle_{\text{conn.}}$. The peak is partially contributed by both the disconnected part and connected part.

In the following sections, we will provide an analytical explanation for these numerical results from the perspective of chaos.

4.2 A first look at late times

To explain the behavior of the transition probability, we first discuss the late-time plateau, and then the linear ramp appearing prior to the plateau.

Let us consider the behavior once the plateau time is reached. Recall the plateau value of the transition probability and the saturation value of Krylov complexity in (2.55). To further estimate their fluctuations a long time after the plateau time t_p , we consider the long-time average of the probability correlation between sites m and n with time lag dt ,

$$\begin{aligned}
& (|\phi_m(\beta + it)|^2 |\phi_n(\beta + i(t + dt))|^2)_\infty - (|\phi_m(\beta + it)|^2)_\infty (|\phi_n(\beta + i(t + dt))|^2)_\infty \\
& \approx \sum_{pq} |\langle E_p | 0 \rangle|^4 |\langle E_q | 0 \rangle|^4 e^{-2\beta(E_p + E_q)} e^{-idt(E_p - E_q)} \psi_m(E_p) \psi_n(E_p) \psi_m(E_q) \psi_n(E_q) \quad (4.2) \\
& = L^{-2} |\langle O_m | e^{-(2\beta + idt)H} | O_n \rangle|^2,
\end{aligned}$$

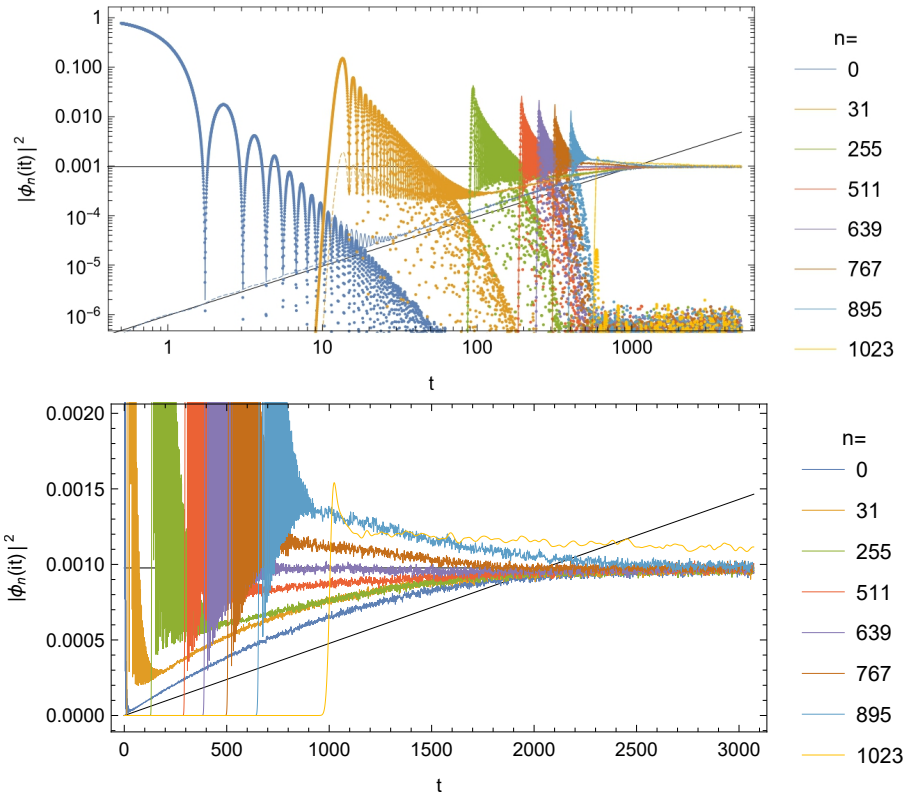


Figure 7. The time evolution of transition probability $|\phi_n(it)|^2$ for different n in chaotic system. We consider the GUE with $L = 1024$ and 4096 realizations. The solid curves, dashed curves, and dots represent the whole transition probability, connected part, and disconnected part respectively. The black lines denote $1/L$ and t/L^2 . The cloud of dots on the bottom is due the finite sampling.

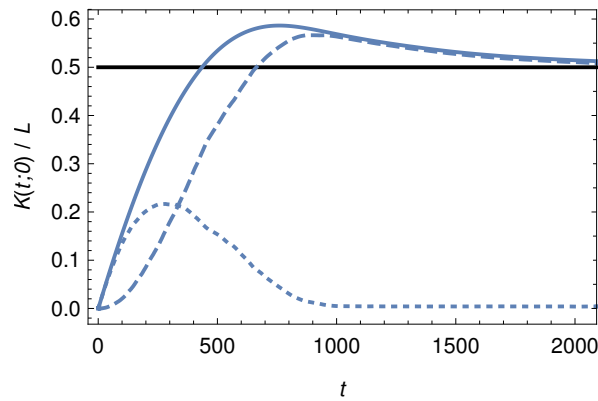


Figure 8. Krylov complexities as functions of time t in chaotic system. We consider the GUE with $L = 1024$ and 128 realizations. The solid curves, dashed curves, and dots represent the whole quantity, connected part, and disconnected part respectively.

where the subscript in $(\dots)_\infty$ denotes the long-time average defined in (2.25). For the first step in (4.2), we use the property that $E_p - E_q = E_{p'} - E_{q'}$ holds only when $p = q, p' = q'$ or $p = p', q = q'$ in a chaotic spectrum [15]. The final result in (4.2) is proportional to the transition probability between sites m and n . From the characteristic curves (2.46), we expect that it reaches a peak when $dt = \pm |y(\epsilon m) - y(\epsilon n)|$, with $y(x)$ the coordinate in (2.45). When $\beta = dt = 0$, the correlation (4.2) is simply $L^{-2}\delta_{mn}$. Thus the local fluctuations take the form

$$[(\Delta |\phi_n|^2)_\infty]^2 = (|\phi_n|^4)_\infty - [(|\phi_n|^2)_\infty]^2 = 1/L^2, \quad (4.3)$$

which is of the same order as $[(|\phi_n|^2)_\infty]^2$ in (2.55). From (4.2), we may easily calculate the fluctuation of Krylov complexity with $\beta = 0$ after saturation,

$$(\Delta K)_\infty^2 = (K^2)_\infty - (K_\infty)^2 = \sum_{m,n=0}^{L-1} mnL^{-2}\delta_{mn} = \frac{L}{3} + O(L^0). \quad (4.4)$$

So the relative fluctuation is $(\Delta K)_\infty/K_\infty \approx 2/\sqrt{3L}$, which is negligible for large L . We conclude that at $\beta = 0$, the transition probability is not self-averaging after saturation, similarly to the SFF [13]. On the other hand, we note that the Krylov complexity is indeed self-averaging after saturation, similar to the spectral complexity [106]. So the relative fluctuation of the transition probability is stronger than the relative fluctuation of the Krylov complexity.

We move on to discussing the ramp before the plateau time. It is well known that the SFF, which is proportional to the survival probability, has a linear ramp. We expect that due to the spectral rigidity, a linear ramp also appears in the transition probability $|\phi_n(\beta + it)|^2$ for $n \neq 0$. For a first look at the linear ramp in the transition probability, we consider the two-point function (3.11) in the GUE in the box approximation [14, 16]

$$\langle \rho(E_1)\rho(E_2) \rangle = \langle \rho(E_1) \rangle \langle \rho(E_2) \rangle + \langle \rho(E) \rangle \left[\delta(s) - \frac{\sin^2(Ls)}{\pi Ls^2} \right], \quad (4.5)$$

where we have sent $E_{1,2} \rightarrow E$ in the connected part as the sine kernel is localized at $s = 0$. Moreover, we also sent $\langle \rho(E) \rangle \rightarrow \langle \rho(0) \rangle = L/\pi$ in the sine kernel, and have given an appropriate normalization to the sine kernel, such that the two-point function reduces to the one-point function $\langle \rho(E_1) \rangle$ if E_2 is integrated out. We calculate the connected generating function

$$\langle Z(\beta + it + it_1)Z(\beta - it + it_2) \rangle_{\text{conn.}} \quad (4.6)$$

$$= \int_{-2}^2 dE \int_{-\infty}^{+\infty} ds \langle \rho(E) \rangle \left[\delta(s) - \frac{\sin^2(Ls)}{\pi Ls^2} \right] e^{-i(2t+t_1-t_2)s/2 - (2\beta+it_1+it_2)E} \quad (4.7)$$

$$\approx \frac{I_1(4\beta + 2it_1 + 2it_2)}{2\beta + it_1 + it_2} \min \left\{ \frac{2t + t_1 - t_2}{4}, 1 \right\}, \quad |t_{1,2}| \ll t \quad (4.8)$$

From (2.53), the connected part of the probability on a given polynomial $\psi(E)$ of low degree is

$$\begin{aligned}
& \frac{1}{L^2} \langle \text{Tr} [\psi(H)e^{-(\beta+it)H}] \text{Tr} [\psi(H)e^{-(\beta-it)H}] \rangle_{\text{conn.}} \\
&= \frac{1}{L^2} \psi(i\partial_{t_1})\psi(i\partial_{t_2}) \langle Z(\beta + it + it_1)Z(\beta - it + it_2) \rangle_{\text{conn.}} \Big|_{t_1=t_2=0} \quad (4.9) \\
&\approx \begin{cases} c_0 + c_1 t, & 0 < t < 2L \\ c_3, & 2L < t \end{cases},
\end{aligned}$$

which exhibits a ramp with nonzero coefficients c_0 and c_1 before a common plateau time $2L$. In App. B.2, we show that the transition probability in a general Gaussian ensemble also exhibits a ramp.

Note however that in (4.9), we neglected two effects:

- When $\psi(E)$ is a n -degree polynomial with $n \lesssim L$, the high-order derivative in (4.9) will be sensitive to the behavior of the generating function (4.6) in the domain of $|t_{1,2}| \sim t$ and the plateau time is also affected.
- The polynomial $\psi_n(E)$ is determined by the Lanczos coefficients, which are in principle determined by the spectrum $\{E_p\}$ in a complicated way. The statistical correlation between the two polynomials and the two spectral density could make other contributions to the connected part of transition probability.

We will take the first effect into account in (4.32) later in Sec. 4.5 .

The second effect is more complicated. In most of the literature, the statistical correlation between the polynomial $\psi_n(E)$ and the density of states $\rho(E)$ is neglected in analytic approaches. We will deal with the second effect step by step: In Sec. 4.3, we will first ignore the statistical correlation of the second effect and calculate the Krylov complexity in the first-order formalism of the continuum limit. The Krylov complexity exhibits a peak already in this approximation. In Sec. 4.4, we will include an obvious effect of the correlation between the polynomial and spectral density, called the *confinement of polynomials*. This leads to a reduced spectral density and approximated polynomials after taking the effect of the confinement of polynomials into account. In Sec. 4.5, we will make use of the reduced spectral density and approximated polynomials and integrate over the spectrum in the transition probability. We find a ramp-to-plateau behavior in its connected part, as expected.

4.3 Krylov complexity in the continuum limit

In this subsection, we derive the complexity in the first-order formalism of the continuum limit, while neglecting the statistical correlation between the polynomial $\psi_n(E)$ and the spectrum $\{E_p\}$. According to [88], and using the solution (2.32), we may define a complexity operator on the energy basis in the continuum limit¹. However, in

¹We thank Souvik Banerjee for helpful discussions on this point.

general, the polynomial in the continuum limit is not normalized to 1, meaning that $(1/L) \int dE |\Psi(E, x)|^2 \rho(E) = 1/b(x)$ and $(1/\epsilon L) \int dx |\Psi(E, x)|^2 = \int dx /(\epsilon L b(x))$. Therefore, we should introduce a normalization factor $\sqrt{b(x)}$ to each $\Psi(E, x)$ before integrating over x . We obtain a complexity operator and total probability on the energy basis in the continuum limit,

$$\begin{aligned} J^{\text{cont.}}(E_1 - E_2) &= \frac{1}{2\epsilon} \int_0^{\epsilon L} dx \, x b(x) (\Psi(E_1, x)^* \Psi(E_2, x) + \Psi(E_2, x)^* \Psi(E_1, x)) \\ &= 2 \int_0^{y(\epsilon L)} dy \, x(y) b(x(y)) \cos((E_1 - E_2)y), \end{aligned} \quad (4.10)$$

$$\begin{aligned} P^{\text{cont.}}(E_1 - E_2) &= \frac{1}{2} \int_0^{\epsilon L} dx \, b(x) (\Psi(E_1, x)^* \Psi(E_2, x) + \Psi(E_2, x)^* \Psi(E_1, x)) \\ &= 2\epsilon \int_0^{y(\epsilon L)} dy \, b(x(y)) \cos((E_1 - E_2)y), \end{aligned} \quad (4.11)$$

where we have taken the symmetric part under exchanging $E_1 \leftrightarrow E_2$. Taking the limit value of the Lanczos coefficients (3.4), we get

$$\Psi(E, x) = \frac{1}{\sqrt{b(x)}} e^{iEy(x)}, \quad b(x) = \sqrt{1 - \frac{x}{\epsilon L}}, \quad y(x) = L \left(1 - \sqrt{1 - \frac{x}{\epsilon L}} \right). \quad (4.12)$$

Then we get the complexity operator and the total probability in the continuum limit

$$J^{\text{cont.}}(s) = \frac{\epsilon}{s^2} \left[(L^2 s^2 + 6) \text{sinc}^2 \frac{Ls}{2} - 6 \right], \quad (4.13)$$

$$P^{\text{cont.}}(s) = \epsilon L \text{sinc}^2 \frac{Ls}{2}, \quad s = E_1 - E_2, \quad (4.14)$$

where we may set the overall factor as $\epsilon = 1/L$ such that $P^{\text{cont.}}(0) = 1$. The completeness relation (2.3) becomes $P^{\text{cont.}}(s)$ in the continuum limit. The asymptotic behaviors of $J^{\text{cont.}}(s)$ are

$$J^{\text{cont.}}(s \rightarrow 0) = \frac{L}{2} - \frac{L^3 s^2}{15} + O(s^3), \quad J^{\text{cont.}}(s \rightarrow \infty) = -\frac{2(\cos(Ls) + 2)}{Ls^2}, \quad (4.15)$$

where the $L/2$ will be the saturation value of the Krylov complexity at $\beta = 0$, as a consequence of our normalization. From (2.54), the expectation value of the Krylov complexity in the continuum limit is

$$K^{\text{cont.}}(t; \beta) = \frac{J^{\text{cont.}}(t; \beta)}{P^{\text{cont.}}(t; \beta)}, \quad (4.16)$$

$$J^{\text{cont.}}(t; \beta) = \frac{1}{L^2} \sum_{pq} J^{\text{cont.}}(E_p - E_q) e^{it(E_p - E_q) - \beta(E_p + E_q)}, \quad (4.17)$$

$$P^{\text{cont.}}(t; \beta) = \frac{1}{L^2} \sum_{pq} P^{\text{cont.}}(E_p - E_q) e^{it(E_p - E_q) - \beta(E_p + E_q)}. \quad (4.18)$$

With the two-point function in the GUE (3.11), we can calculate them in the ensemble average

$$\langle J^{\text{cont.}}(t; \beta) \rangle = \frac{1}{L^2} \int_{-2}^2 dE \int_{-\infty}^{+\infty} ds J^{\text{cont.}}(s) \left\{ \rho_{\text{sc}}(E)^2 + \rho_{\text{sc}}(E) \left[\delta(s) - \frac{\sin^2(\pi \rho_{\text{sc}}(E) s)}{\rho_{\text{sc}}(E) (\pi s)^2} \right] \right\} e^{its - 2\beta E}, \quad (4.19)$$

$$\langle P^{\text{cont.}}(t; \beta) \rangle = \frac{1}{L^2} \int_{-2}^2 dE \int_{-\infty}^{+\infty} ds P^{\text{cont.}}(s) \left\{ \rho_{\text{sc}}(E)^2 + \rho_{\text{sc}}(E) \left[\delta(s) - \frac{\sin^2(\pi \rho_{\text{sc}}(E) s)}{\rho_{\text{sc}}(E) (\pi s)^2} \right] \right\} e^{its - 2\beta E}. \quad (4.20)$$

where we have replaced the energies in the spectral density by their average E , since both $J^{\text{cont.}}(s)$ and $P^{\text{cont.}}(s)$ are localized around $s = 0$ with a width $\sim 20/L$. We will use the box approximation (4.5) by replacing $\rho_{\text{sc}}(E) \rightarrow \rho_{\text{sc}}(0)$ in the sine kernel. The final result at $\beta = 0$ is

$$\langle K^{\text{cont.}}(t; 0) \rangle = L \begin{cases} \frac{3\pi u^5 - 15\pi u^4 + 20\pi u^3 + 320u^3 - 960u^2 + 640u + 7\pi}{-10\pi u^3 + 30\pi u^2 - 320u + 10\pi + 320}, & u < 1 \\ \frac{3u^5 - 15u^4 + 20u^3 + 15u + 7}{-10u^3 + 30u^2 + 30u + 10}, & 1 \leq u < 2 \\ \frac{-3u^5 + 45u^4 - 260u^3 + 720u^2 - 945u + 519}{10u^3 - 90u^2 + 270u - 150}, & 2 \leq u < 3 \\ \frac{1}{2}, & 3 \leq u \end{cases}, \quad u = \frac{t}{L} \quad (4.21)$$

whose configuration is plotted in Fig. 9. $\langle K^{\text{cont.}}(t; 0) \rangle$ reaches a peak of value $0.75L$ at time $t \approx 0.7L$ and nearly saturates to $0.5L$ when $t > L$. We further separate the contribution of the disconnected and connected parts of two-point function in the integrand of (4.19) and show them in Fig. 9. We see that the linear growth as well as the peak are mainly contributed by the disconnected part and the saturation is contributed by the connected part in this continuum limit. While the peak in the numeric Krylov complexity is partially contributed by the connected part, as shown in Fig. 8. The reason for discrepancy is that we neglect the fluctuation in the polynomial $\psi_n(E)$ coming from the fluctuation on levels. Those fluctuation transform some contribution from disconnected part to the connected part. We will come to this point later.

Furthermore, $\langle K^{\text{cont.}}(t; 0) \rangle$ grows as $\frac{7\pi}{10(32+\pi)}L + \frac{16(640+27\pi)}{5(32+\pi)^2}t + O(t^2)$ initially, which are not reliable when compared to the early-time behavior in Sec. (3). They are affected by the loss of orthogonality, *e.g.* $\int dE \rho(E) \Psi(E, x) * 1 \neq 0$ for $x \neq 0$, which is an artifact of the continuum limit.

4.4 Confinement of polynomials

In the following two subsections, we give the details on finding a good approximation to the polynomials and also the transition probability. The reader just interested in the result for the peak of the Krylov complexity may jump to Sec. 4.6.

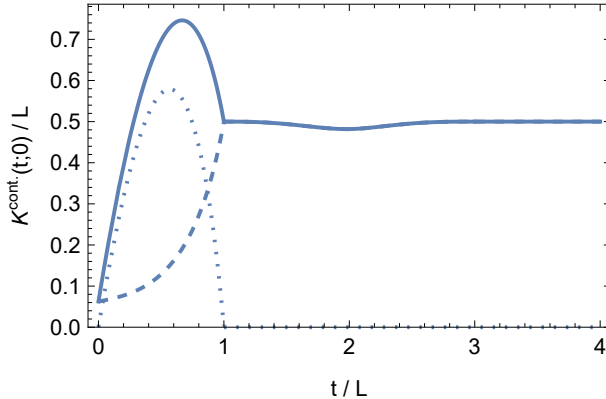


Figure 9. The Krylov complexity as a function of time in the continuum limit at $\beta = 0$. The solid curves, dashed curves, and dotted curves represent the whole quantities, connected parts, and disconnected parts respectively.

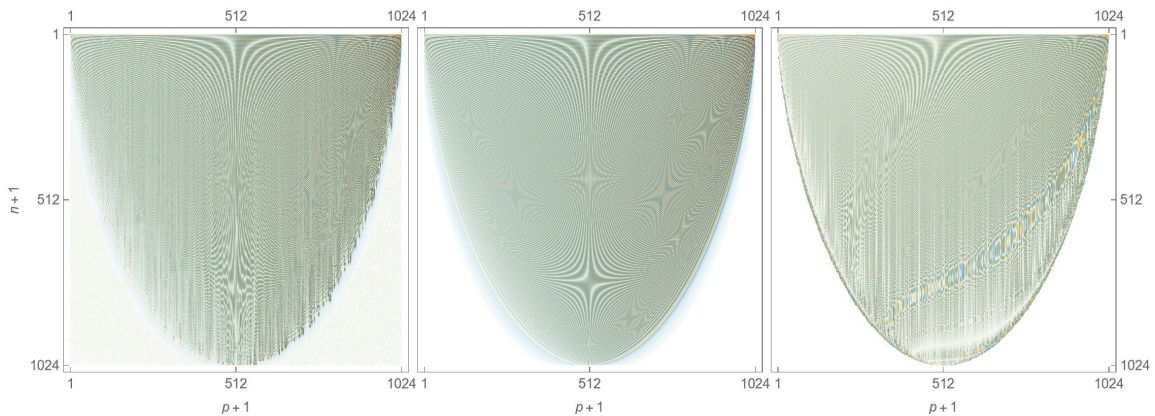


Figure 10. Polynomials $\psi_n(E_p)$ as functions of n and p , where $L = 1024$. Left: the polynomials in the Krylov space of TFD state in one realization of the GUE. Middle: the polynomials from (3.4). Right: the deformed Chebyshev polynomials (4.29) on a GUE spectrum within $-2\sqrt{1-n/L} < E_p < 2\sqrt{1-n/L}$.

We will include the most significant statistical correlation between the polynomial $\psi_n(E)$ and the spectrum $\{E_p\}$. For clarity, we will show the dependence on the spectrum $\{E\} = \{E_0, E_1, \dots, E_{L-1}\}$ explicitly for the polynomial $\psi(E') = \psi_n(E'; \{E\})$. Instead of considering $\psi_n(E'; \{E\})$ as a function of a continuous energy E' , we focus on its dependence on the discrete levels $E' = E_p$ with $p = 0, 1, \dots, L-1$. We show that ψ is a function $\psi_n(E_p; \{E\})$ for a realization of the GUE. This is displayed on the left of Fig. 10. An important feature is that the $\psi_n(E_p; \{E\})$ almost vanishes for $|E_p| \gtrsim 2\sqrt{1-n/L}$, which is different from the profile of $\psi_n(E'; \{E\})$ in the continuous domain of spectrum, namely $[-2, 2]$ in our convention. In other words, $\psi_n(E; \{E\})$ passes its zeros on those $E_p \notin [-2\sqrt{1-n/L}, 2\sqrt{1-n/L}]$. We call this the confinement of $\psi_n(E_p; \{E\})$. It is

an important consequence of the statistical correlations between the polynomial $\psi_n(E; \{E\})$ and the spectrum $\{E\}$, that we will consider below.

The confinement of $\psi_n(E_p; \{E\})$ is due to the decrease of b_n as a sequence of n , as explained as follows. Let us send b_n of the corresponding n in \mathbf{L} to 0 and denote the resulting matrix as $\tilde{\mathbf{L}}$. The spectra of \mathbf{L} and $\tilde{\mathbf{L}}$ are close. Since $\tilde{\mathbf{L}} = \mathbf{L}^{(n)} \oplus \mathbf{R}^{(L-n)}$, where $\mathbf{L}^{(n)}$ and $\mathbf{R}^{(L-n)}$ are the upper-left block and the lower-right block respectively, the whole spectrum is the union of the spectra of $\mathbf{L}^{(n)}$ and $\mathbf{R}^{(L-n)}$. So, the spectral density $\rho(E)$ in (3.7) may be divided into two parts

$$\rho(E) = \bar{\rho}^{(n)}(E) + \rho^{(L-n)}(E), \quad (4.22)$$

where the spectral density $\bar{\rho}^{(n)}(E)$ of $\mathbf{L}^{(n)}$ and the spectral density $\rho^{(L-n)}(E)$ of $\mathbf{R}^{(L-n)}$ are given by the integrals (3.7) with modified bounds $\int_0^{n/L} dx$ and $\int_{n/L}^1 dx$, which are normalized to n and $L - n$, respectively.

Recall that $p_n(E) = \det(E - \mathbf{L}^{(n)})$ from (2.8). So, $p_n(E_p)$ automatically vanishes on the spectrum of $\mathbf{L}^{(n)}$. Then we can reduce the summation

$$\sum_p p_n(E_p; \{E\}) f(E_p) \approx \sum_p^{(L-n)} p_n(E_p; \{E\}) f(E_p), \quad (4.23)$$

where the $\sum_p^{(L-n)}$ is taken on the spectrum of $\mathbf{R}^{(L-n)}$ and $f(E_p)$ is an arbitrary function of E_p . We will assume (4.26) to be the ensemble average of the density of the levels E_p with nonzero $\psi_n(E_p; \{E\})$. The ensemble average means evaluating any quantity on the measure of the spectrum $\int DE = \int dE_0 dE_1 \cdots dE_{L-1} P(E_0, E_1, \cdots, E_{L-1})$, where $P(E_0, E_1, \cdots, E_{L-1})$ for $\tilde{\beta}$ -ensemble is given as (B.9) in App. B. After taking the confinement of polynomials into account, we neglect the other correlation between the polynomial and spectral density in the ensemble average. So (4.23) become

$$\int DE \sum_p \psi_n(E_p; \{E\}) f(E_p) \approx \int_{-2\sqrt{1-n/L}}^{2\sqrt{1-n/L}} dE \langle \psi_n(E) \rangle \langle \rho^{(L-n)}(E) \rangle f(E). \quad (4.24)$$

where $\langle \psi_n(E) \rangle$ and $\langle \rho^{(L-n)}(E) \rangle$ are the polynomials and the reduced spectral density respectively in ensemble average. Since $b_n = 0$ in this trick of replacing \mathbf{L} by $\tilde{\mathbf{L}}$, the original norm $\prod_{m=1}^n b_m^2$ vanishes. We will introduce the normalization factor in the reduced spectral density $\langle \rho^{(L-n)}(E) \rangle$, so that the norm in ensemble average is normalized to unity

$$\int DE \frac{1}{L} \sum_p \psi_n(E_p; \{E\})^2 \approx \frac{1}{L} \int_{-2\sqrt{1-n/L}}^{2\sqrt{1-n/L}} dE \langle \psi_n(E) \rangle^2 \langle \rho^{(L-n)}(E) \rangle = 1. \quad (4.25)$$

We will approximate the reduced spectral density $\langle \rho^{(L-n)}(E) \rangle$ and the polynomials $\langle \psi_n(E) \rangle$ in the following way. We take the limit value (3.4) and find that the spectral

density from $\mathbf{R}^{(L-n)}$ is also a semicircle law,

$$\rho_{\text{sc}}^{(L-n)}(E) = \frac{L}{2\pi(1-n/L)} \sqrt{4\left(1 - \frac{n}{L}\right) - E^2} \Theta\left(4\left(1 - \frac{n}{L}\right) - E^2\right), \quad (4.26)$$

where we have introduced an additional normalization factor $1/(1-n/L)$ so that the reduced spectral density is normalized to L . This normalization will lead to the normalization (4.25) with a proper polynomial $\langle\psi_n(E)\rangle$.

We will approximate the polynomials in the following two ways. First, we can approximate the polynomial $\langle\psi_n(E)\rangle$ in the continuum limit in the second-order formalism. We consider $\epsilon = 1/L$, finite n/L , and large L . Inserting the limit value (3.4) into the wave equation (2.45), we find $V = O(1/L^4)$ which is negligible. With the boundary conditions (2.47), we obtain the ‘‘polynomial’’ in the continuum limit

$$\psi_n^{\text{cont.}}(E) = \begin{cases} (-1)^{n/2} \frac{\cos(EL(1-\sqrt{1-n/L}))}{(1-n/L)^{1/4}}, & \text{even } n \\ (-1)^{(n-1)/2} \frac{\sin(EL(1-\sqrt{1-n/L}))}{(1-n/L)^{1/4}}, & \text{odd } n, \end{cases} \quad (4.27)$$

which coincides with the real part and imaginary part of (4.12). The frequency $L(1 - \sqrt{1-n/L})$ in (4.27) is just the coordinate y corresponding to n in (2.45). The transformation (2.14) from E to t on (4.27) gives a wave function $\phi_n(it)$. Since (4.27) is not a polynomial with finite degree and only contains two frequencies $\pm L(1 - \sqrt{1-n/L})$, the wave function is localized around the characteristic curve $t = \pm L(1 - \sqrt{1-n/L})$ in (2.46), which is different from the numerical result in Fig. 6, where the waves have long tails.

However, we find that $\psi_n^{\text{cont.}}(E)$ is normalized to

$$\frac{1}{L} \int \psi_n^{\text{cont.}}(E)^2 \rho_{\text{sc}}^{(L-n)}(E) = \frac{1}{2\sqrt{1-n/L}} \left[{}_0\tilde{F}_1 \left(; 2; -4 \left(n + L \left(\sqrt{1-n/L} - 1 \right) \right)^2 \right) + 1 \right] \quad (4.28)$$

with the reduced spectral density $\rho_{\text{sc}}^{(L-n)}(E)$ in (4.26), where ${}_0\tilde{F}_1$ is the regularized confluent hypergeometric function. The normalization approaches $1/(2\sqrt{1-n/L})$ when $n \gg 1$. Consequently, we will multiply (4.27) with $\sqrt{2}(1-n/L)^{1/4}$ when we use it to calculate the transition probability in (4.32).

Second, the polynomial satisfying the orthogonality relation (2.2) with respect to the measure given by the semi-circle law (3.8) is given by the Chebyshev polynomials of the second kind $U_n(E/2)$. However, we show that $U_n(E/2)$ are not the polynomials we need since they are given by constant Lanczos coefficients $a_n = 0$, $b_n = 1$ (see (D.3) in App. D). Here, the Lanczos coefficients are those given in (3.4). So, compared to the polynomials given by the Lanczos coefficients (3.4) with a plateau for $n \ll L$ and a descent for $n \lesssim L$, the Chebyshev polynomials $U_n(E/2)$ for $n \ll L$ only.

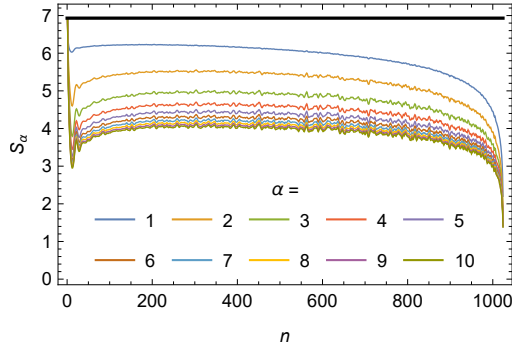


Figure 11. The α -Renyi entropy S_α of the Krylov basis $\{|O_n\rangle\}_{n=0}^{L-1}$ from the maximally entangled state in the GUE of $L = 1024$ and 128 realizations. The black line denotes $\log L$.

We may modify the Chebyshev polynomials based on the above discussion of the matrix $\tilde{\mathbf{L}}$. To this end, we approximate the sub-matrix $\mathbf{L}^{(n)}$ by replacing the Lanczos coefficients with their square mean value. For the limit value (3.4), we set $a_m \rightarrow 0$ and $b_m \rightarrow \bar{b}_n$, $\forall m \in [0, n-1]$ in $\mathbf{L}^{(n)}$. We may rescale the energy $E \rightarrow E/\bar{b}_n$ in the Chebyshev polynomial $U_n(E/(2\bar{b}_n))$ such that the original domain of Chebyshev polynomials is rescaled to the domain $E \in [-2\bar{b}_n, 2\bar{b}_n]$. Recall that the spectral domain of $\mathbf{R}^{(L-n)}$ is $[-2\sqrt{1-n/L}, 2\sqrt{1-n/L}]$. We will choose $\bar{b}_n = b_n = \sqrt{1-n/L}$ such that $U_n(E/(2\sqrt{1-n/L}))$ is approximately orthogonal to other $U_{n'}(E/(2\sqrt{1-n/L}))$ with $n' \sim n$ on the measure of $\rho_{\text{sc}}^{(L-n)}(E)$.

However, we immediately encounter the following problem. $U_n(E/(2\sqrt{1-n/L}))$ around $E = 0$ is proportional to $\exp(\pm iE(n+1)/(2\sqrt{1-n/L}))$. Again, by transforming E to t , we find a shock wave propagating along $t = \pm(n+1)/(2\sqrt{1-n/L})$ that is very different from the characteristic curve $t = \pm L(1 - \sqrt{1-n/L})$ found in the continuum limit for large n . To fix this problem, recalling that the spectral domain has been rescaled, we tune the degree of the Chebyshev polynomial to match the characteristic curve $t = \pm L(1 - \sqrt{1-n/L})$. The resulting polynomial is

$$\langle \psi_n(E) \rangle \approx \psi_n^{\text{Cheb.}}(E) = U_{d_n} \left(\frac{E}{2b_n} \right), \quad (4.29)$$

$$d_n = 2L(1 - \sqrt{1-n/L})\sqrt{1-n/L}, \quad b_n = \sqrt{1-n/L},$$

which will be confined in $E \in [-2\sqrt{1-n/L}, 2\sqrt{1-n/L}]$. The normalization coefficient h_n is determined by (4.25). The degree d_n approaches n for small n and 0 for $n = L$. We compare the polynomials (4.29) to the numerical result in Fig. 10 and also compare them to the numerical statistics result in Fig. 18 in App. B.

In App. B, we compare the $|\langle \psi_n(E) \rangle|^j \langle \rho^{(L-n)}(E) \rangle$ we adopt above to the histogram of the spectrum $\{E_p\}$ with weight $|\langle \psi_n(E_p) \rangle|^j$ from the numeric Lanczos algorithm (2.6).

A physical consequence of the confinement property discussed above is the decrease of entanglement in the Krylov basis from the maximally entangled state. Given

a state $|O_n\rangle$ in the Krylov basis, we expand it on the equal-energy states as $|O_n\rangle = (1/\sqrt{L}) \sum_{p=0}^{L-1} \psi_n(E_p) |E_p, E_p\rangle$, take the partial trace on \mathcal{H}_R , obtain a reduced density matrix in \mathcal{H}_L , and calculate the α -Renyi entropy $S_\alpha = \left[\log(\sum_{p=0}^{L-1} |\psi_n(E_p)|^{2\alpha} / L) \right] / (1-\alpha)$. We display the α -Renyi entropies for all the states in the Krylov basis in the GUE in Fig. 11. Recall that $|O_0\rangle$ is the maximally entangled state, whose α -Renyi entropy is $S_\alpha = \log L, \forall \alpha$. When $n \gg 1$, after the recurrence (2.9) with random levels, the resulting Krylov state $|O_n\rangle$ has a nonuniform and random component on the equal-energy basis $|E_p, E_p\rangle$ with $E_p \in [-2\sqrt{1-n/L}, 2\sqrt{1-n/L}]$. This confinement of the spectrum leads to the decrease of entanglement for increasing n . In particular, when $1 \ll n \ll L$, the dimension of the subspace spanned by the equal-energy basis within $[-2\sqrt{1-n/L}, 2\sqrt{1-n/L}]$ is exponentially large. So, first the entanglement decreases slowly. When n approaches L , the dimension of the subspace shrinks quickly and the entanglement decreases quickly as well.

4.5 Chaos in transition probability

Here we consider the transition probability for $n \lesssim L/2$. Similarly to the analysis of (4.24), we consider the confinement of polynomials and neglect other correlations between the polynomials and spectral the density. We find the transition probability

$$\begin{aligned} & \langle |\phi_n(\beta + it)|^2 \rangle \tag{4.30} \\ & \approx \left| \frac{1}{L} \int dE \langle \psi_n(E) \rangle \langle \rho^{(L-n)}(E) \rangle e^{-(\beta+it)E} \right|^2 + \frac{1}{L^2} \int dE \langle \psi_n(E) \rangle^2 \langle \rho^{(L-n)}(E) \rangle e^{-2\beta E} \\ & - \frac{1}{L^2} \int dE ds \langle \psi_n(E + s/2) \rangle \langle \psi_n(E - s/2) \rangle \langle \rho^{(L-n)}(E) \rangle \frac{\sin^2(\pi \rho_{\text{sc}}(E)s)}{\rho_{\text{sc}}(E)(\pi s)^2} e^{-2\beta E - its} + \dots \end{aligned}$$

We only consider the correlation between the arguments of the polynomials in the connected part of (4.30), and neglect the correlation between the spectra of the polynomials. We discuss this neglected correlation in App. B.

The first term of (4.30) contributes to the rise-slope. From our numerical results in Fig. 6, we expect a sharp shock and a long tail on the Krylov chain, which corresponds to a sharp rise and a long slope along the real-time axis. The continuum limit fails to describe the long slope since it is localized at a frequency. We will adopt the deformed Chebyshev polynomial (4.29) in the first term of (4.30) and the reduced semicircle law (4.26). The first term is the absolute square of

$$\begin{aligned} \langle \phi_n(\tau) \rangle & \approx \frac{1}{2\pi(1-n/L)} \int_{-2\sqrt{1-n/L}}^{2\sqrt{1-n/L}} dE U_{d_n} \left(\frac{E}{2\sqrt{1-n/L}} \right) e^{-\tau E} \sqrt{4 \left(1 - \frac{n}{L}\right) - E^2} \\ & = (-1)^n \frac{d_n + 1}{\tau \sqrt{1-n/L}} I_{d_n+1} \left(2\tau \sqrt{1 - \frac{n}{L}} \right) \tag{4.31} \end{aligned}$$

with $\tau = \beta + it$. So the transition probability $\langle |\phi_n(it)|^2 \rangle$ rises as $(1 - n/L)^{d_n} t^{2d_n} / \Gamma(d_n + 1)^2$ initially, reaches its first peak around the time $L(1 - \sqrt{1 - n/L})$, and then decays as $(d_n + 1)^2 / [\pi t^3 (1 - n/L)^2]$ over time.

The second term of (4.30) contributes to the plateau. From the normalization (4.25), the plateau value is $1/L$.

The third term of (4.30) contributes to the ramp-up behavior for $n \lesssim L/2$. The product $\langle \psi_n(E + s/2) \rangle \langle \psi_n(E - s/2) \rangle$ is an even and oscillating function of s with a frequency of order n . Under the Fourier transformation of the level difference s , the oscillation will shift the time t by some scales of n , which is not negligible when n is comparable to L . To estimate this effect analytically for $n \gg 1$, we employ the polynomial in the continuum limit (4.27) and the reduced semicircle law (4.26) with a normalization factor of $2\sqrt{1 - n/L}$ from (4.28). To get a simple expression, we adopt the box approximation by sending $\rho_{\text{sc}}(E) \rightarrow \rho_{\text{sc}}(0)$ in the sine kernel. The sum of the second and third terms for even n at $\beta = 0$ is given by

$$\begin{aligned} & \frac{1}{L} - \frac{\pi}{4L(L-n)} \int_{-2\sqrt{1-n/L}}^{2\sqrt{1-n/L}} dE \int_{-\infty}^{\infty} ds \sqrt{4\left(1 - \frac{n}{L}\right) - E^2} \frac{\sin^2(Ls)}{(\pi s)^2} e^{-its} \quad (4.32) \\ & \quad \times \cos\left(2L(E + s/2)(1 - \sqrt{1 - n/L})\right) \cos\left(2L(E - s/2)(1 - \sqrt{1 - n/L})\right) \\ & = \frac{1}{4L^2} \left[\min\left(\left|t - L(1 - \sqrt{1 - n/L})\right|, 2L\right) + \min\left(\left|t + L(1 - \sqrt{1 - n/L})\right|, 2L\right) \right]. \end{aligned}$$

For odd n , we obtain the same result. The function is plotted in Fig. 12. The plateau value is always $1/L$, and the time dependence can be understood by the movement of the two min terms for different n . Each of them, as a function of t , is given by an upside-down triangle centered on the characteristic curve $t = \pm L(1 - \sqrt{1 - n/L})$, with a width of $4L$. When $n = 0$, the two triangles, centered at $t = 0$, stack up to form a larger triangle, which corresponds to the ramp $t/(2L^2)$ of survival probability before the plateau time $t_p = 2L$. When $n > 0$, the two triangles move apart due to the oscillation of the polynomials on s . Then a step appears between the centers of the two triangles, whose height is $(1 - \sqrt{1 - x})/(2L)$ and width is $2L(1 - \sqrt{1 - n/L})$. The ramp behaves as $t/(2L^2)$ when $L(1 - \sqrt{1 - n/L}) < t < L(1 + \sqrt{1 - n/L})$, and as $t/(4L^2)$ when $L(1 + \sqrt{1 - n/L}) < t < L(3 - \sqrt{1 - n/L})$. Thus, the plateau time is $t_p = L(3 - \sqrt{1 - n/L})$.

The dip time, which is the time when the ramp surpasses the slope, is given by $t_d \approx \sqrt[4]{2/\pi} \sqrt{L(n+1)}$ for $n \lesssim L/2$. Therefore, the ramp region of the transition probability $\langle |\phi_n|^2 \rangle$ lasts for $\sqrt{(L-n)L}$ long.

As we will show in the next subsection, the transition probability in a non-chaotic system have short ramp regions and different plateau times. So, the above ramp-to-plateau behavior characterizes the chaos in the Krylov space.

In Fig. 13, we compare the numerical results with the analytical results obtained from (4.31) and (4.32). The rise-slope behaviors match well until n approaches L , but

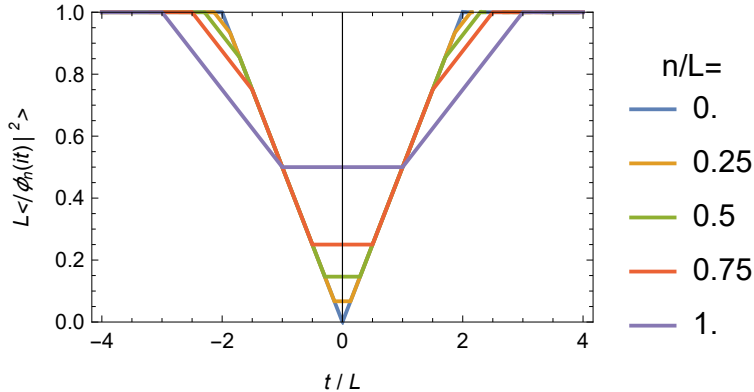


Figure 12. The ramp(-up)-plateau in the continuum limit (4.32) as functions of t/L for different n/L . We specially plot the negative axis of t/L to show how the step in $-1 + \sqrt{1 - n/L} < t/L < 1 - \sqrt{1 - n/L}$ emerges.

the ramp-up behaviors obtained from (4.32) are smaller than the numerical results due to neglecting the fluctuations from the polynomials, as discussed in (B.27) of App. B.

For $n \gtrsim L/2$, we are unable to reproduce the behavior of the transition probability analytically, including the rise-slope and ramp-down. This is because the Lanczos coefficients exhibit strong fluctuations at large $n \gtrsim L/2$, as shown in Fig. 2. Consequently, the polynomial $\psi_n(E_p; \{E\})$ receives strong fluctuations from the spectrum $\{E\}$, and the correlation between the two polynomials is not negligible. Such fluctuations in polynomials lead to strong fluctuating phenomena in the transition probability for $n \gtrsim L/2$.

In the single realization shown in Fig. 3, the shock and tail of the transition probability fluctuate at large n . In the ensemble average shown in Fig. 7, the rise-slope and ramp-down behavior are mainly contributed from the connected part, which implies strong fluctuations in each realization. We discuss the origin of the ramp-down behavior based on the strong fluctuation of the slope in App. C.

A direct consequence of the ramp-up behavior in the transition probability is that nearly all observables in an m -dimensional Krylov subspace spanned by $\{|O_n\rangle\}_{n=0}^{m-1}$ with $m \lesssim L/2$ will exhibit ramps after the dip time of $|\phi_m|^2$. For example, the m -site probability $P^{(m)}$ defined as

$$P^{(m)} = \sum_{n=0}^{m-1} |\phi_n|^2, \quad (4.33)$$

ramps up after its slope in chaotic systems, as shown in Fig. 14.

4.6 The peak of Krylov complexity

We can now explain the peak observed in the Krylov complexity, which appears slightly before the plateau time t_p and much later than the dip time t_d for small n .

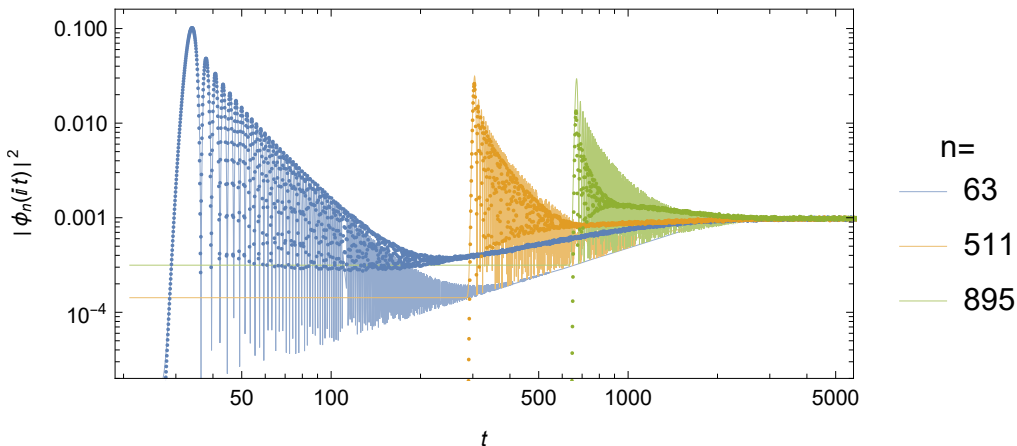


Figure 13. The transition probability $|\phi_n(it)|^2$ for $n = 63, 511, 895$ as functions of time t , where $L = 1024$. The dots are the numerical results in the average of 4096 realizations and the curves are the analytical results from (4.31) and (4.32).

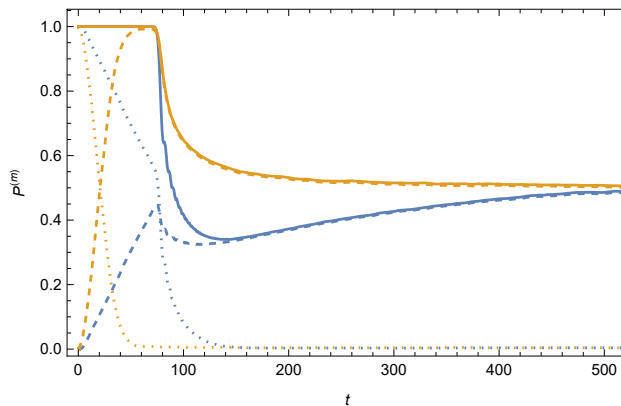


Figure 14. m -site probability $P^{(m)}$ as function of time t in the chaotic systems (blue curves) and non-chaotic systems (orange curves) with $L = 256$, $m = L/2$, $\beta = 0$, and 128 realizations. The solid curves, dashed curves, and dots represent the whole quantity, connected part, and disconnected part respectively.

The transition probability for all small n is in the ramp region, while the transition probability for all large n is in the rise-slope region. Considering the weight n in the Krylov complexity, the former is negligible while the latter dominates. Thus, the observed peak in the Krylov complexity is essentially the weighted combination of peaks in the rise-slope region of the transition probability at large n .

More precisely, we consider the saturated case where the shock reaches the n -th site at time t , and the transition probability before the n -th site is in its ramp region, i.e., $\langle |\phi_m(it)|^2 \rangle \gtrsim t/(2L^2)$ with $0 \leq m < n$. Due to probability conservation, which is equal to 1 at $\beta = 0$, we have $\langle |\phi_n(it)|^2 \rangle \lesssim 1 - tn/(2L^2)$. The shock is described

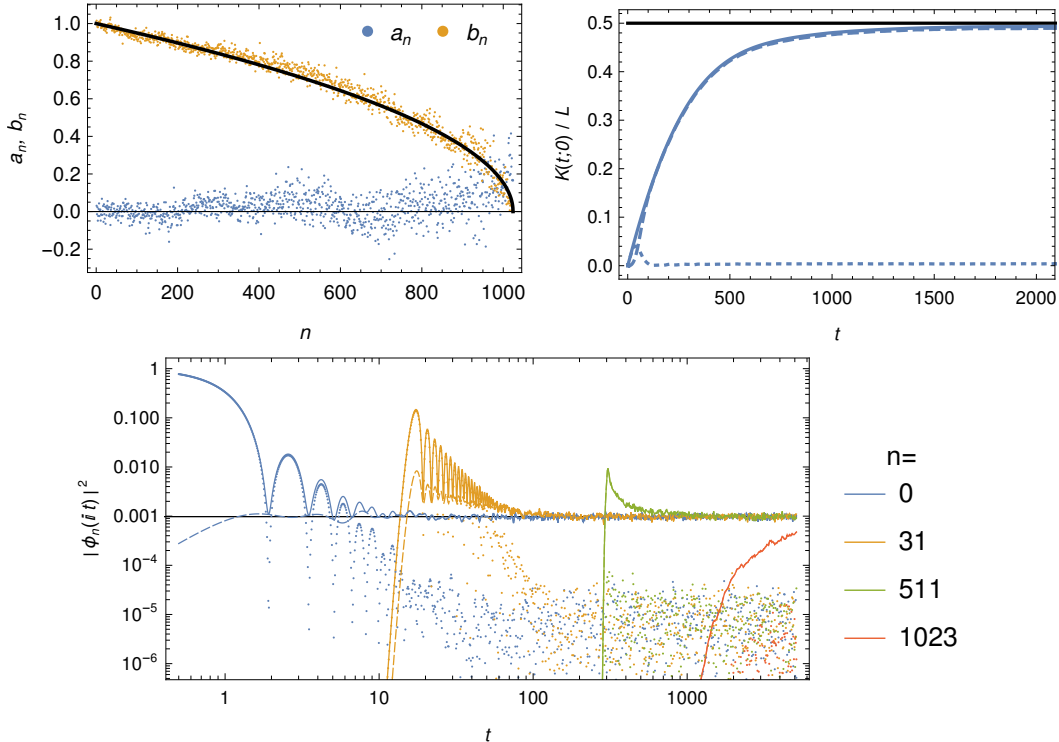


Figure 15. The Lanczos coefficients (upper-left), Krylov complexity (upper-right), and transition probability (lower) of the non-chaotic spectra with $L = 1024$. In the last two plots, the solid curves, dashed curves, and dots represent the whole quantities, connected parts, and disconnected parts, respectively, over 128 realizations. The black line in the last plot denotes $1/L$.

by (3.5). Then, the Krylov complexity is bounded above by

$$K \leq n(t) \left(1 - \frac{tn(t)}{2L^2} \right) + \frac{n(t)(n(t) - 1)t}{4L^2} = \frac{t(2L - t)(2L^3 - Lt(2t + 1) + t^3)}{2L^4}, \quad t \leq L, \quad (4.34)$$

which has a peak around $t = 0.62L$.

We can also explain why the linear growth of Krylov complexity is not a result of chaos before its peak time. The dip times of the transition probabilities for different n are mismatched, so the rise-slope of the transition probability in the shock wave always covers the ramps of other transition probabilities.

5 Non-chaotic spectrum

As a comparison, following the example given in [66], we can consider an uncorrelated spectrum whose density satisfies the same semicircle law (3.8). Technically, we randomly sample the energies individually from the spectra in the GUE with dimension L . We calculate the Lanczos coefficients, transition probability, and Krylov

complexity numerically, as shown in Fig. 15. The m -site probability is shown in Fig. 14.

The Lanczos coefficients approach the limit value (3.4) in ensemble average in consistence with the semi-circle law and (3.6). But they have strong fluctuation especially at large n .

To study the behavior of transition probability, we consider the two-point function of uncorrelated spectrum

$$\langle \rho(E_1)\rho(E_2) \rangle = \rho(E)\delta(E_1 - E_2) + \frac{L-1}{L} \langle \rho(E_1) \rangle \langle \rho(E_2) \rangle, \quad (5.1)$$

where the spectral density in ensemble average obeys the semi-circle law $\langle \rho(E) \rangle = \rho_{\text{sc}}(E)$. Similarly, considering the confinement and then decorrelating the polynomials and the spectral density, we obtain the SFF and the transition probability respectively

$$\langle |Z(\beta + it)|^2 \rangle = L + \frac{L(L-1) |I_1(2\beta + 2it)|^2}{\beta^2 + t^2}, \quad (5.2)$$

$$\langle |\phi_n(\beta + it)|^2 \rangle \approx \frac{1}{L^2} \int dE e^{-2\beta E} \langle \psi_n(E)^2 \rho^{(L-n)}(E) \rangle + \frac{L-1}{L} |\langle \phi_n(\beta + it) \rangle|^2 \quad (5.3)$$

$$= \frac{1}{L} + \frac{L-1}{L} |\langle \phi_n(\beta + it) \rangle|^2 \quad \text{when } \beta = 0. \quad (5.4)$$

The first terms will give a plateau and there is no ramp. Since the Lanczos coefficients have strong fluctuations, the wave function $\phi_n(it)$, which is initially localized at $n = 0$, quickly diffuses as it propagates, as observed in [1] as well. Thus, when n is not too large, the transition probability $\langle |\phi_n(it)|^2 \rangle$ exhibits rise-slope-plateau behaviors without any ramp, as shown in Fig. 15. The plateau value is universally $1/L$, but the plateau time, *i.e.*, the time when its slope become smaller than $1/L$, highly depends on n and is much earlier than $2L$. When n is increasing and approaching L , the peak between the rise and the slope decays quickly and even ceases to exist. Finally, when the transition probability only gradually rises and approaches the plateau $1/L$ from below. The decay or even absence of the peak in the transition probability for $n \lesssim L$ is the result of probability conservation. Consider the time when $\langle |\phi_n(it)|^2 \rangle$ is rising, due to the absence of ramp, all the $\langle |\phi_m(it)|^2 \rangle$ with $m \ll n$ have entered their plateau regions and all the $\langle |\phi_m(it)|^2 \rangle$ with $m \lesssim n$ have entered their slope region. In both cases, $\langle |\phi_m(it)|^2 \rangle \geq 1/L$. From (2.18), we get $\langle |\phi_n(it)|^2 \rangle < 1 - n/L$, which decreases with increasing n and approaches its plateau value $1/L$ when $n \lesssim L$. Due to the absence of ramp in the transition probability, we will not find any ramp in m -site observable (4.33), as shown in Fig. 14. Following the strong fluctuations in the Lanczos coefficients, the polynomials $\psi_n(E_p; \{E\})$ will get a stronger fluctuation at larger n via the spectrum $\{E\}$. So we observe that the connected parts of the transition probability $\langle |\phi_n|^2 \rangle_{\text{conn.}}$ become dominated at large n .

Since the Lanczos coefficients are still around the limit value (3.4). By plugging the the SFF (5.2) into the Ehrenfest theorem (2.22) and doubly integrating over the time, we obtain the Krylov complexity at the early time. In particular at $\beta = 0$,

$$K(t; 0) \approx {}_1F_2 \left(-\frac{1}{2}; 1, 2; -4t^2 \right) - 1 \rightarrow \begin{cases} t^2, & t \ll 1 \\ \frac{16}{3\pi}t, & 1 \ll t \ll L \end{cases}, \quad (5.5)$$

which agrees with the numerical result displayed in Fig. 15. This linear growth has the same rate as the growth in RMT at early times. We thus confirm that, when the reference state is the maximally entangled state, the linear growth of Krylov state complexity does not characterize chaos in the spectrum ².

However, at late times, the Krylov complexity from non-chaotic spectrum gradually slows down and reaches a plateau from below at $t \gtrsim L$, without going through a peak (see Fig. 15), which is in contrast to the Krylov complexity in the GUE at late times (see Fig. 8). The absence of the peak in the Krylov complexity is due to the absence of the ramp in the transition probability. Recall that $\langle |\phi_n(it)|^2 \rangle < 1 - n/L$ due to the early plateau time and probability conservation, which bounds the complexity contributions from probability at large n . To describe this in detail, let us consider the saturated case, in which the shock reaches the n -th site at time t , i.e. $\langle |\phi_n(it)|^2 \rangle = 1 - n/L$ and $\langle |\phi_m(it)|^2 \rangle = 1/L$ with $0 \leq m < n$. With shock (3.5), the Krylov complexity is bounded from above by

$$K \leq n(t) \left(1 - \frac{n(t)}{L} \right) + \frac{n(t)(n(t) - 1)}{2L} = \frac{L}{2} \left(1 - \left(1 - \frac{t}{L} \right)^4 \right) + O(L^0), \quad t \leq L \quad (5.6)$$

The bound monotonically grows from 0 to $(L - 1)/2$ when n goes from 0 to $L - 1$ or t goes from 0 to L , and then it saturates. We may thus rule out the peak exceeding the saturated value $L/2$ in the Krylov complexity.

6 The SYK model

Here we show that the universal rise-slope-ramp-plateau behavior also appears in the SYK model with quartic or higher fermions interactions. The SYK _{q} model describes N Majorana fermions with q -fermion random coupling, namely

$$H = i^{\frac{q}{2}} \sum_{1 \leq j_1 < j_2 < \dots < j_q \leq N} J_{j_1, \dots, j_q} \chi_{j_1} \dots \chi_{j_q}, \quad \langle J_{j_1, \dots, j_q}^2 \rangle = \frac{(q-1)! J_0^2}{N^{q-1}}, \quad (6.1)$$

and anti-commutation relation $\{\chi_j, \chi_k\} = \delta_{jk}$. We specify the value of J_0 so that the Lanczos coefficient b_1 is equal to one, $b_1 = 1$.

²We distinguish chaos in spectrum from chaos characterized by the exponential decay of the OTOC, which is related to operators and locality [15, 40].

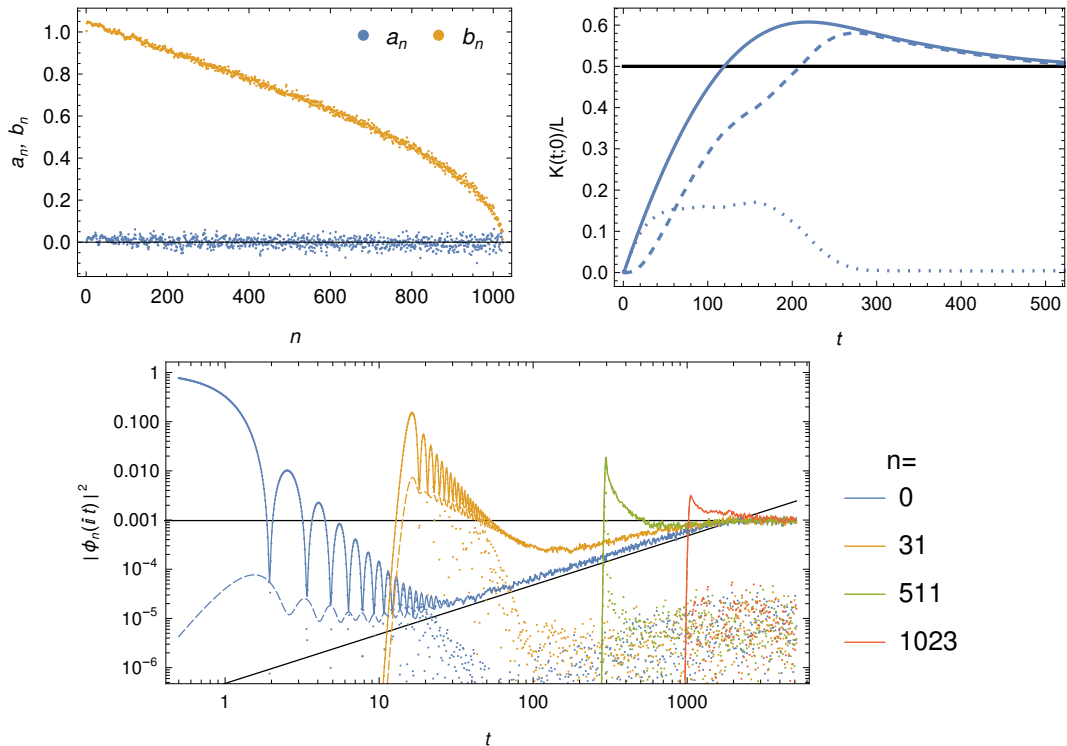


Figure 16. The Lanczos coefficients (upper-left), Krylov complexity (upper-right), and transition probability (lower) of the SYK₄ model with $N = 22$, $L = 1024$, and 128 realizations. In the last two plots, the solid curves, dashed curves, and dots represent the whole quantities, connected parts, and disconnected parts, respectively. The black lines in the last plot denote $1/L$ and $t/(2L^2)$.

The SYK_q model with $q \geq 4$ has the same level spacing distribution as the RMT [9, 10, 14]. The particle-hole symmetry determines the class of RMT statistics (GOE, GUE, and GSE) of each charge parity sector. For the GUE, we will consider $N \bmod 8 = 2$ or 6 , where the spectrum consists of even and odd parity sectors which are mapped to each other by the particle-hole symmetry. Each sector corresponds to the GUE with dimension $L = 2^{N/2-1}$.

For the SYK model with $q = 4$, the spectral density is Gaussian law rather than semi-circle law [8, 10]. We show the Lanczos coefficients, Krylov complexity, and transition probability at $\beta = 0$ in Fig. 16. The Lanczos coefficients b_n decrease linearly for $n \ll L$ and decrease like $\sim \sqrt{1 - n/L}$ for $n \lesssim L$. The transition probability exhibits the rise-slope-ramp-plateau behavior with ramp $\sim t/(2L^2)$, a common plateau time $t_p \approx 2L$ and a common plateau value $1/L$. The connected contributions to the rise-slope are more obvious. Due to the existence of ramp in the transition probability, the Krylov complexity has a peak after its linear growth and before the plateau time.

The SYK₂ model is a many-body model of $N/2$ free Dirac fermions filling random

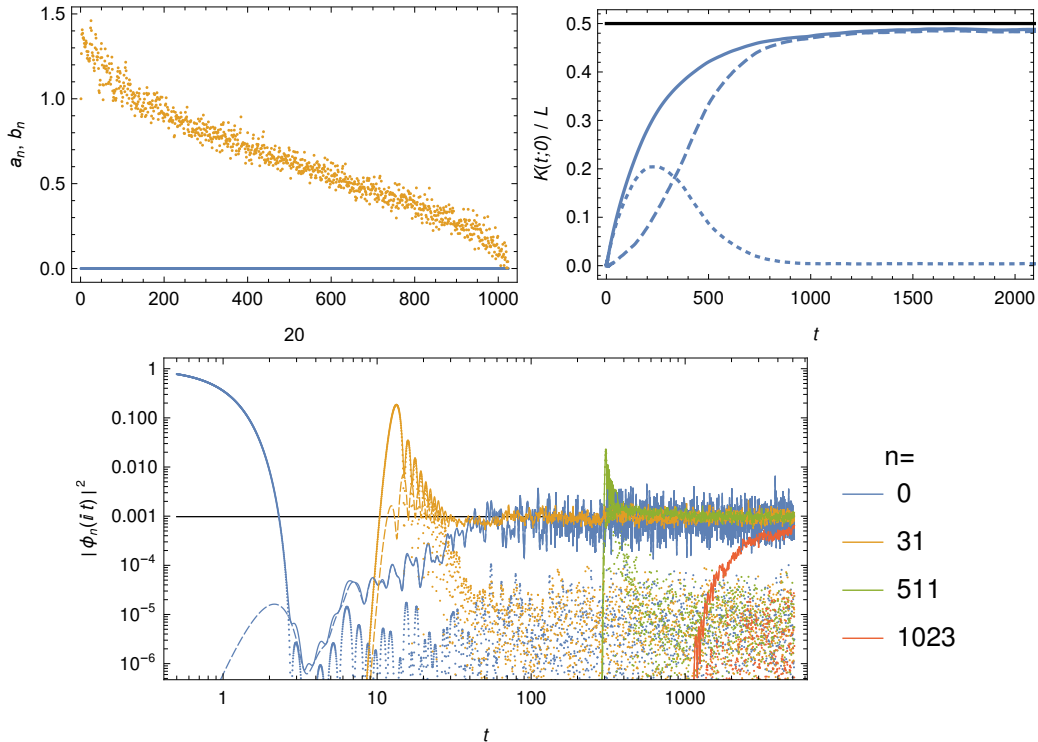


Figure 17. The Lanczos coefficients (upper-left), Krylov complexity (upper-right), and transition probability (lower) of the SYK₂ model with $N = 20$, $L = 1024$, and 128 realizations. In the last two plots, the solid curves, dashed curves, and dots represent the whole quantities, connected parts, and disconnected parts, respectively. The black line in the last plot denotes $1/L$.

matrix single-particle energy levels. The model is integrable and non-chaotic. The many-body spectral density satisfies a Gaussian law. The levels have weak correlation and repulsion and its SFF has an exponential ramp instead of a linear ramp [108]. The dimension of the Krylov space is $L = 2^{N/2}$. We show the Lanczos coefficients, Krylov complexity, and transition probability at $\beta = 0$ in Fig. 17. The Lanczos coefficients b_n decrease faster than linearly for $n \ll L$ and $a_n = 0$ due to the exact reversal symmetry of the spectrum. The transition probability exhibits the rise-slope-ramp-plateau behavior with a negligible ramp at finite n , a n -dependent plateau time t_p and a common plateau value $1/L$. Due to the absent of a long ramp in the transition probability, the Krylov complexity does not have a peak.

7 Conclusion and outlook

We have studied the Krylov complexity in random matrix theory by mapping it to an effective Krylov spin chain model. Under the reasonable assumption of neglecting the statistical correlation between wavefunction and spectra, we find that the Krylov

complexity satisfies an Ehrenfest theorem, in which the spectral form factor serves as a force to drive the complexity to grow. For random matrix theory, this also enables us to derive an analytical approximation of Krylov complexity, in terms of spectral complexity (3.10). The analytical expression matches well with numerical calculations up to the linear growth region, while its asymptotic late-time value deviates from the actual saturation value. We attribute this deviation to the fact that neglecting the fluctuation of Lanczos coefficient is not valid at late times, as revealed by Fig. 7. This deviation also shows the fundamental difference between the saturation of Krylov complexity and the saturation of spectral complexity at late times: the former relies on the discreteness of the spectrum (2.55), while the latter relies on level rigidity.

For early times, our generalized version of the Ehrenfest theorem is valid for the linear growth region of both chaotic and non-chaotic systems. This implies that the linear growth of complexity is not sufficient to discriminate chaotic and non-chaotic systems.

This further motivated us to study the quantum dynamics in the Krylov basis in general. We find that the transition amplitude, properly defined in a two-copy Hilbert space, shows a universal rise-slope-ramp-plateau behavior as function of time. The linear ramp behavior is a robust indicator for chaotic systems, similarly to the spectral form factor. Therefore, unlike global observables that span over all of the Krylov basis, such as the Krylov complexity, any observable defined in the subspace of the Krylov space can reveal the linear ramp behavior that is unique for chaotic systems. Our study of the transition probability also explains the existence (absence) of the peak in the Krylov complexity in chaotic (non-chaotic) systems discussed in [1]. Our analysis thus reveals a close relation between chaotic spectra and the Krylov state complexity.

In this context, there remain some open questions for the future.

First, the saturation value predicted by the Ehrenfest theorem is not accurate, and the error stems from the approximation that we neglect the fluctuations of the Lanczos coefficients in Eqs. (3.4) and (3.9). It will be interesting to improve the approximation by including more statistical correlations between the Lanczos coefficients and the Krylov wavefunction. A similar improvement can be obtained for the Krylov wavefunction ϕ_n at chain sites with large $n \sim L$.

Second, in addition to the Ehrenfest theorem presented in this paper, further theorems in quantum mechanics may provide useful approximations or constraints for observables on the Krylov chain. For instance, the Robertson uncertainty relation provides a dispersion bound for Krylov complexity [109]. It will be interesting to investigate this bound in each region of Krylov state complexity discussed in this paper.

Third, for $n \gtrsim L/2$, the statistical correlation between the two polynomials in the transition probability makes the ramp-down behavior at late times difficult to

analyze. In the numerical simulation, we observe that the late-time evolution of the transition probability is governed by diffusion rather than propagation. It would be more straightforward to describe the ramp-down behavior by writing down a diffusion equation for the Krylov chain.

Fourth, going beyond random matrix ensembles, it would be interesting to study Krylov state complexity in the SYK model [110–112] and in holographic models such as JT gravity [11, 106], as well as in lattice models or spin models to benchmark the universal behavior studied in our paper.

Finally, let us highlight the fact that (2.54) provides an analytical expression for the Krylov complexity for the TFD state. This may serve as a starting point for constructing the gravity dual of Krylov complexity [113]. As we show in Sec. 4, the connected part of the Krylov complexity plays an important role for its peak and saturation structure at time scales comparable to the dimension of the Hilbert space. This may be relevant in particular for describing the late-time evolution of black holes, where higher genus effects should be taken into account at finite N in holography [106].

Acknowledgements

We are grateful to Vijay Balasubramanian, Souvik Banerjee, Pawel Caputa, Adolfo del Campo, Pratik Nandy, and Dario Rosa for discussions. The research of J. E. and Z.-Y. X. is funded by DFG through the Collaborative Research Center SFB 1170 ToCoTronics, Project-ID 258499086—SFB 1170, as well as by Germany’s Excellence Strategy through the Würzburg-Dresden Cluster of Excellence on Complexity and Topology in Quantum Matter - ct.qmat (EXC 2147, project-id 390858490). Z.-Y. X. also acknowledges support from the National Natural Science Foundation of China under Grants No. 11875053 and No. 12075298. S.-K.J is supported by a startup fund at Tulane University.

A Imaginary time evolution

For imaginary time evolution, we consider the following continuum limit

$$x_n = \epsilon n, \quad \varphi(\tau, x_n) = (-1)^n \phi_n(\tau), \quad b(x_n - \epsilon/2) = b_n, \quad a(x) = a_n, \quad (\text{A.1})$$

with a small spacing ϵ such that Eq. (2.15) becomes

$$\partial_\tau \varphi = \epsilon^2 b \varphi'' + \epsilon^2 b' \varphi' + (2b - a) \varphi + O(\epsilon^4). \quad (\text{A.2})$$

In the continuum limit, the Ehrenfest theorem (2.22) becomes

$$\partial_t^2 J = \frac{1}{\epsilon^2} \partial_t^2 \int |\varphi|^2 x dx = \int dx \left[2(b^2)' |\varphi|^2 - 2a'b |\varphi|^2 + \epsilon^2 b b'' (|\varphi|^2)' + \epsilon^2 (b^2)' |\varphi'|^2 \right] \quad (\text{A.3})$$

where the last two terms in the integrand may be neglected in the small ϵ limit.

To further write it into a typical Schrödinger equation in the continuous coordinates, we introduce a new wave function $\tilde{\varphi}(\tau, y) = b(x)^{1/4}\varphi(\tau, x)$ on coordinate $y = y(x)$ with $dy = dx/(\epsilon\sqrt{b})$, and arrive at the following Schrödinger equation

$$-\partial_\tau \tilde{\varphi} = -\partial_y^2 \tilde{\varphi} + \tilde{V} \tilde{\varphi}, \quad (\text{A.4})$$

with the potential

$$\tilde{V}(y) = \frac{B''(y)}{4B(y)} - \frac{3B'(y)^2}{16B(y)^2} - 2B(y) + A(y) = \frac{\epsilon^2 b''(x)}{4} - \frac{\epsilon^2 b'(x)^2}{16b(x)} - 2b(x) + a(x) \quad (\text{A.5})$$

where $A(y) = a(x)$, $B(y) = b(x)$, $A'(y) = \partial_y A(y)$, $B'(y) = \partial_y B(y)$. The expectation value of operator O transforms to

$$\langle O \rangle = \sum_n O_n |\tilde{\varphi}_n|^2 = \frac{1}{\epsilon} \int_0^{\epsilon L} O(x) |\tilde{\varphi}(x)|^2 dx = \int_{y(0)}^{y(\epsilon L)} O(x(y)) |\tilde{\varphi}(y)|^2 dy. \quad (\text{A.6})$$

We can read out another Ehrenfest theorem on the coordinate y and real time $t = \text{Im}\tau$,

$$\partial_t^2 \langle y \rangle = -\langle \tilde{V}'(y) \rangle. \quad (\text{A.7})$$

However, the Krylov complexity $\langle xL \rangle$ is not directly related to $\langle y \rangle$.

B Krylov approach in ensemble average

B.1 Krylov complexity in ensemble average

As explain in the main text, to construct the Krylov space of the maximally entangled state $|0\rangle$, we can consider non-degenerate spectrum $\{E_p\}_{0 \leq p \leq L-1}$. The Krylov space is spanned by the states $\mathcal{L}^n |0\rangle$ for $0 \leq n \leq L-1$. The components of the n -th state on the energy basis of \mathcal{L} are the n -th rows of the Vandermonde matrix

$$\mathbf{V} = \{E_p^n\}_{0 \leq n, p \leq L-1} \quad (\text{B.1})$$

times $1/\sqrt{L}$. So the Krylov basis $|O_n\rangle$ is obtain from the orthogonalization of \mathbf{V} , namely

$$\Psi = \{L^{-1/2}\psi_n(E_p)\}_{0 \leq n, p \leq L-1} = \mathbf{C}\mathbf{V}, \quad \Psi\Psi^T = \Psi^T\Psi = \mathbf{I} \quad (\text{B.2})$$

where \mathbf{C} is a lower-triangular matrix and \mathbf{I} is the identity matrix. From the moments and Hankel matrix

$$\mu_j = \sum_p E_p^j, \quad \mathbf{A}^{(m,n)} = \{\mu_{i+j}\}_{0 \leq i \leq m-1, 0 \leq j \leq n-1}. \quad (\text{B.3})$$

one can also derive the orthogonal polynomials by

$$\psi_n(E) = \frac{1}{\sqrt{h_n} \det \mathbf{A}^{(n,n)}} \det \begin{pmatrix} \mathbf{A}^{(n,n+1)} \\ 1 & E & E^2 & \dots & E^n \end{pmatrix}. \quad (\text{B.4})$$

If the spectrum is symmetric, one can also divide the Lanczos coefficients from the Hankel determinant

$$D_n = \det \mathbf{A}^{(n,n)}, \quad D_0 = 1, \quad b_n^2 = \frac{D_{n-1} D_{n+1}}{D_n^2} \quad (\text{B.5})$$

The the transition probability and Krylov complexity are respectively

$$|\phi_n|^2 = \frac{(\Psi \mathbf{F} \Psi^T)_{nn}}{\text{Tr} \mathbf{F}}, \quad K = \frac{\text{Tr}[\mathbf{K} \Psi \mathbf{F} \Psi^T]}{\text{Tr} \mathbf{F}}, \quad (\text{B.6})$$

where the evolution matrix and complexity matrix are respectively

$$\mathbf{F} = \{e^{-\tau E_p - \tau^* E_q}\}_{0 \leq p, q \leq L-1}, \quad \mathbf{K} = \{n \delta_{mn}\}_{0 \leq m, n \leq L-1}. \quad (\text{B.7})$$

In an ensemble average, they become

$$\langle |\phi_n|^2 \rangle = \int DE \frac{(\Psi \mathbf{F} \Psi^T)_{nn}}{\text{Tr} \mathbf{F}}, \quad \langle K \rangle = \int DE \frac{\text{Tr}[\mathbf{K} \Psi \mathbf{F} \Psi^T]}{\text{Tr} \mathbf{F}}, \quad (\text{B.8})$$

For $\tilde{\beta}$ -ensemble, the measure of the spectrum is

$$\int DE = \frac{1}{Z_{\tilde{\beta}}} \int dE_0 dE_1 \dots dE_{L-1} \exp \left(-\frac{\tilde{\beta} L}{4} \sum_{0 \leq p \leq L-1} E_p^2 \right) \prod_{0 \leq p < q \leq L-1} |E_p - E_q|^{\tilde{\beta}} \quad (\text{B.9})$$

which is normalized to 1 and we have rescaled the potential such that the domain of spectrum is $[-2, 2]$ in expectation. We will work at the GUE ($\tilde{\beta} = 2$) for simplicity. It can be solved with the oscillator wave functions

$$\varphi_n(x) = \frac{1}{\sqrt{2^n n! \sqrt{\pi}}} \exp \left(-\frac{x^2}{2} \right) H_n(x) \quad (\text{B.10})$$

where $H_n(x)$ is the Hermite polynomial. By using the kernel

$$K_n(x, y) = \sum_{m=0}^{n-1} \varphi_m(x) \varphi_m(y) \quad (\text{B.11})$$

one can write down the one point function and two point function

$$\langle \rho(E) \rangle = K_L(x, x), \quad \langle \rho(E_1, E_2) \rangle = K_L(x, y)^2. \quad (\text{B.12})$$

In the large L limit, they become the semi-circle law and sine kernel

$$\langle \rho(E) \rangle = \frac{L}{2\pi} \sqrt{4 - E^2}, \quad \langle \rho(E_1, E_2) \rangle = \text{sinc}(\pi L(E_1 - E_2)). \quad (\text{B.13})$$

Since $\psi_n(E_p)$ is a complicated function of the spectrum of degree n , the ensemble average of probability $\langle |\phi_n|^2 \rangle$ is a complicated summation of maximally $2n$ -point function and difficult to be solve analytically. So we will approximate $\psi_n(E_p)$ by the polynomials $\psi_n(E)$ given by the limit value (3.4) and take its confinement into account.

B.2 General linear ramp from Gaussian ensemble

Similar to the SFF, the ramp in the transition probability does not rely on the specific sine kernel. Here, we work at $\beta = 0$ for simplicity. Since the $\psi_n(E)$ in $|\phi_n|^2$ is a n -degree polynomial of E , we can consider the generating function in the Gaussian ensemble average $\langle \dots \rangle$, namely

$$\langle \text{Tr}[e^{-it_1 H}] \text{Tr}[e^{it_2 H}] \rangle = \int D\rho \int dE_1 dE_2 \rho(E_1) \rho(E_2) e^{-it_1 E_1 + it_2 E_2} e^{-S[\rho]}, \quad (\text{B.14})$$

where $S[\rho]$ is an effective action of spectral density ρ from Gaussian ensemble. The saddle point of S is the semi-circle ρ_s . Considering fluctuation $\rho = \rho_s + \delta\rho$ and expanding S around its saddle, one find the quadratic term [15]

$$\delta S = -L^2 \int^\Lambda dE_1 dE_2 \delta\rho(E_1) \delta\rho(E_2) \log |E_1 - E_2| = \frac{L^2}{\Lambda^2} \sum_n \delta\rho_n \delta\rho_{-n} \frac{\text{Si}(n\pi)}{n\pi}, \quad (\text{B.15})$$

where $\delta\rho_n = \int^\Lambda dE \delta\rho(E) e^{iEs_n}$ is the Fourier transformation from a finite domain of spectrum $E \in [-\Lambda/2, \Lambda/2]$ to discrete $s_n = 2\pi n/\Lambda$ with $n \in \mathbb{N}$, $\text{Si}(x) = \int_0^x (\text{sinc } t) dt$, and $\text{sinc}(x) = (\sin x)/x$. Then the connected part of the generating function is related to the two-point function of $\delta\rho$, namely

$$\int D\delta\rho \sum_{mn} \delta\rho_m \delta\rho_n \text{sinc}(\pi m + \Lambda t_1/2) \text{sinc}(\pi n - \Lambda t_2/2) e^{-\delta S} \quad (\text{B.16})$$

$$= \frac{L^2}{\Lambda^2} \sum_n \frac{n\pi}{\text{Si}(n\pi)} \text{sinc}(-n\pi + \Lambda t_1/2) \text{sinc}(n\pi - \Lambda t_2/2) \quad (\text{B.17})$$

$$\approx \frac{L^2 \sqrt{t_1 t_2}}{\pi \Lambda} \text{sinc}(\Lambda(t_1 - t_2)/2), \quad \text{when } |t_1 - t_2| \ll 1/\Lambda. \quad (\text{B.18})$$

By replacing $t_1 \rightarrow t + t_1$ and $t_2 \rightarrow t - t_2$ and letting $|t_{1,2}| \ll t$, we obtain a linear ramp on t in the connected part of the generating function

$$\langle \text{Tr}[e^{-i(t+t_1)H}] \text{Tr}[e^{i(t-t_2)H}] \rangle_{\text{conn.}} \approx \frac{L^2 t}{\pi \Lambda} \text{sinc}(\Lambda(t_1 + t_2)/2). \quad (\text{B.19})$$

which has a similar behavior as the generating function (4.6) in the main text. Thus, following (4.9) by taking the derivative of (B.19) with respect to $t_{1,2}$, we will obtain a ramp.

B.3 Confinement in ensemble average

Based on our discuss on the confinement of $\psi_n(E_p)$ in the main text, we cut the Lanczos coefficients \mathbf{L} into two part $\tilde{\mathbf{L}} = \mathbf{L}^{(n)} \oplus \mathbf{R}^{(L-n)}$ and separate the summation over the spectrum into two parts

$$\sum_p = \sum_p^{(n)'} + \sum_p^{(L-n)}, \quad (\text{B.20})$$

where $\sum_p^{(n)'}$ sum over the levels from $\mathbf{L}^{(n)}$ and $\sum_p^{(L-n)}$ sum over the levels from $\mathbf{R}^{(L-n)}$. So, the spectral density could be approximately divided into two parts (4.22).

In ensemble average, we consider the following one point function

$$\left\langle \sum_p^{(L-n)} \delta(E' - E_p) \right\rangle = \langle \rho^{(L-n)}(E') \rangle. \quad (\text{B.21})$$

Given a function $f(E)$, we approximate the ensemble average of $\sum_p \psi_n(E_p)^j f(E_p)$ as

$$\begin{aligned} \int DE \sum_p \psi_n(E_p; \{E\})^j f(E_p) &\approx \int DE \sum_p^{(L-n)} \psi_n(E_p; \{E\})^j f(E_p) \\ &= \int DE \int dE' \psi_n(E'; \{E\})^j f(E') \sum_p^{(L-n)} \delta(E' - E_p) \\ &\approx \int dE' \langle \psi_n(E') \rangle^j f(E') \langle \rho^{(L-n)}(E') \rangle \end{aligned} \quad (\text{B.22})$$

with power $j = 1, 2$. At the first step, we break \mathbf{L} into $\tilde{\mathbf{L}}$ and only sum over the spectrum of $\mathbf{R}^{(L-n)}$ part following (4.23). At the third step, we consider the average separately by neglecting the correlation between each term.

In Sec. 4.4, we consider the limit value of Lanczos coefficient (3.4), approximate $\langle \rho^{(L-n)}(E) \rangle$ by $\rho_{\text{sc}}^{(L-n)}(E)$, approximate $\langle \psi_n(E) \rangle$ by the deformed Chebyshev polynomial (4.29), and normalize the polynomial in (4.25). Taking $f(E_p) = \delta(x - E_p)$ and $j = 1, 2, 3$, we get the distribution of E_p with weight $\psi_n(E_p)^2$. We compare the approximated expressions $\rho_{\text{sc}}^{(L-n)}(E)$ and $\langle \psi_n(E) \rangle^2 \rho_{\text{sc}}^{(L-n)}(E)$ to the numerical statistics in Fig. 18. We see that the approximation on $\langle \rho^{(L-n)}(E) \rangle$ works well. The polynomials have closed moving average and oscillation frequency even at $n = L/2$ but their amplitudes and the edges behaviors are different. The numeric statistics give weaker oscillation mainly due to two reasons:

- The approximation on \mathbf{L} by $\tilde{\mathbf{L}}$ will affect the levels slightly such that some levels from $\mathbf{L}^{(n)}$ skip the zero points of $\psi_n(E_p)^2$.

- The fluctuation of the polynomials $\psi_n(E_p)$ will also shift the phase of the oscillation. The mismatch between the phases in different realizations will suppress the oscillation in average.

The numeric statistic has smooth edges while the approximation has cliffy edges, where the discrepancy is due to our hard cut in breaking \mathbf{L} to $\tilde{\mathbf{L}}$. The comparison in Fig. 18 shows that the normalization in (4.26) is a good approximation for the spectral density with weight $|\psi_n(E)|^j$.

For two-point functions of the reduced spectral density, the selection in $\sum_p^{(L-n)}$ will not change the correlation between levels. We consider the following two point function

$$\begin{aligned} & \left\langle \sum_{p,q}^{(L-n)} \delta(E' - E_p) \delta(E'' - E_q) \right\rangle \\ &= \langle \rho^{(L-n)}(E') \rangle \langle \rho^{(L-n)}(E'') \rangle + \langle \rho^{(L-n)}(\bar{E}) \rangle \left[\delta(s) - \frac{\sin^2(\pi \langle \rho(\bar{E}) \rangle s)}{\langle \rho(\bar{E}) \rangle (\pi s)^2} \right] \end{aligned} \quad (\text{B.23})$$

We have introduced the improved sine kernel in [16] to include the correlation between E_p, E_q in the two delta functions. Since the sine kernel is localized in $-1/L < E_p - E_q < 1/L$, we assume that E_p and E_q belongs to the summation $\sum_{p \neq q}^{(L-n)}$ or not simultaneously. So, only one reduced spectral density $\langle \rho^{(L-n)}(\bar{E}) \rangle$ is present with the sine kernel. If we integrate out E'' , we reproduce the one point function (B.21). We can also use the box approximation by replacing $\langle \rho(\bar{E}) \rangle \rightarrow \langle \rho(0) \rangle$ in the sine kernel [16].

Similarly, by assuming the decorrelation between polynomials and spectral density after considering the confinement of $\psi_n(E_p)$, we approximate the transition probability as

$$\begin{aligned} & \langle |\phi_n(\tau)|^2 \rangle \\ &= \frac{1}{L^2} \int DE \sum_{p,q} \psi_n(E_p; \{E\}) \psi_n(E_q; \{E\}) e^{-\tau E_p - \tau^* E_q} \end{aligned} \quad (\text{B.24})$$

$$\approx \frac{1}{L^2} \int DE \sum_p^{(L-n)} \psi_n(E_p; \{E\})^2 e^{-2\beta E_p} \quad (\text{B.25})$$

$$\begin{aligned} & + \frac{1}{L^2} \int DE dE' dE'' \psi_n(E'; \{E\}) \psi_n(E''; \{E\}) e^{-\tau E' - \tau^* E''} \sum_{p \neq q}^{(L-n)} \delta(E' - E_p) \delta(E'' - E_q) \\ & \approx \frac{1}{L^2} \int dE \langle \psi_n(E) \rangle^2 \langle \rho^{(L-n)}(E) \rangle e^{-2\beta E} \\ & + \frac{1}{L^2} \int dE' dE'' \langle \psi_n(E') \rangle \langle \psi_n(E'') \rangle \langle \rho^{(L-n)}(E') \rangle \langle \rho^{(L-n)}(E'') \rangle e^{-\tau E' - \tau^* E''} \\ & - \frac{1}{L^2} \int dE' dE'' \langle \psi_n(E') \rangle \langle \psi_n(E'') \rangle \langle \rho^{(L-n)}(\bar{E}) \rangle \frac{\sin^2(\pi \langle \rho(\bar{E}) \rangle s)}{\langle \rho(\bar{E}) \rangle (\pi s)^2} e^{-2\beta \bar{E} - its} \end{aligned} \quad (\text{B.26})$$

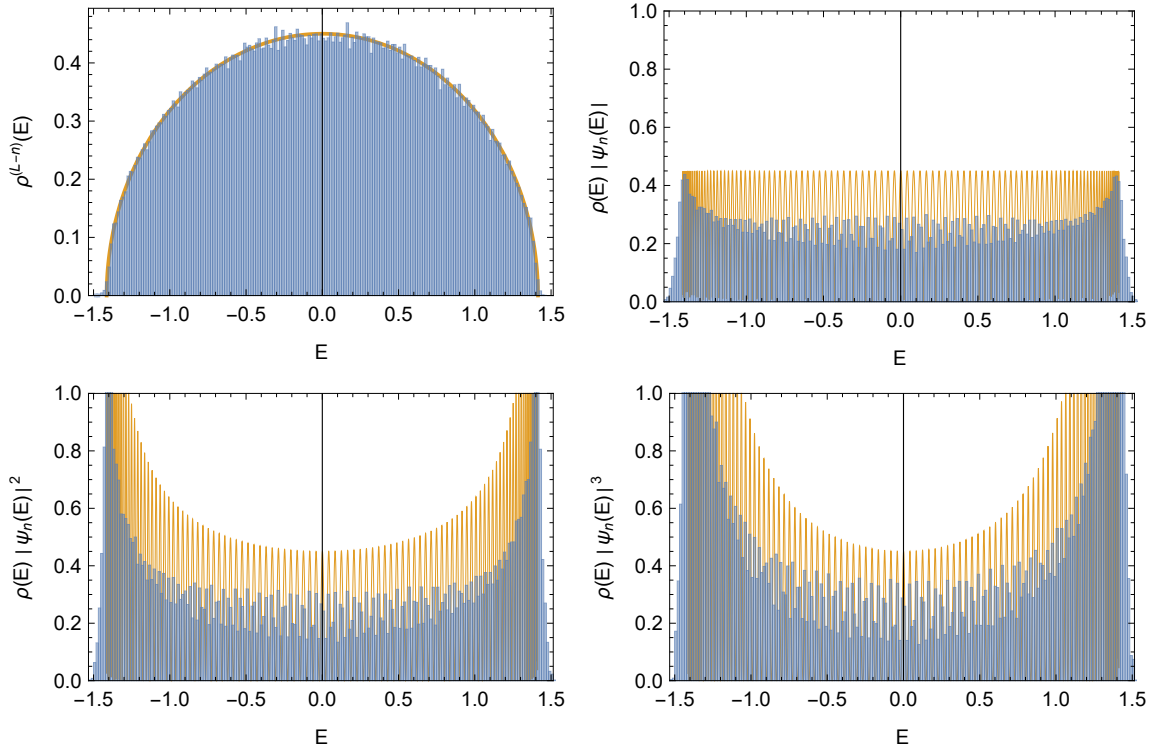


Figure 18. The reduced spectral density $\rho^{(L-n)}(E)$ (upper-left) and the spectral density $\rho(E)$ with weights $|\psi_n(E)|^j$ (others), where $j = 1, 2, 3$, $L = 256$, $n = 128$. The blue bins show the histograms of the average density functions over 1024 realizations of the GUE. The orange curves show the reduced semicircle law (4.26) and deformed Chebyshev polynomial (4.29). We use bin width $1/64$ in the histograms to show the oscillation.

where $\tau = \beta + it$, $\bar{E} = (E' + E'')/2$, and $s = E' - E''$. At the last step, we neglect the spectral correlation between the polynomials and delta functions. Although the sine kernel is localized in $-1/L < s < 1/L$, we can not identify the E' and E'' in the two polynomials, since their product, as a function of s , oscillates quickly when $n \lesssim L$.

We have dropped the complicated correlation between the spectra in polynomials, namely

$$\frac{1}{L^2} \int DE dE' dE'' \psi_n(E'; \{E\}) \psi_n(E''; \{E\}) e^{-\tau E' - \tau^* E''} \langle \rho^{(L-n)}(E') \rangle \langle \rho^{(L-n)}(E'') \rangle, \quad (\text{B.27})$$

which we are unable to calculate. However, we will see its contribution to the transition probability numerically.

Finally, we will approximate the ensemble averages in (B.26) with the reduced spectral density $\rho_{sc}^{(L-n)}(E)$ in (4.26) and the deformed Chebyshev polynomial $\psi_n^{\text{Cheb.}}(E)$ in (4.29) or the polynomial at continuum limit $\psi_n^{\text{cont.}}(E)$ in (4.27).

C Ramp down

In Fig. 13, for $n \gtrsim L/2$, we observe that the ramp down region of the numerical result is inside the slope region of the analytical result. A possible explanation of the ramp down behavior is as follows. The ramp down for $n \gtrsim L/2$ is originated from the slope but with strong fluctuation from the polynomials. The fluctuation in the polynomials leads to phase fluctuation in the oscillation of the slope. For example, we can imagine a phase φ fluctuation in $\left| I_{d_{n+1}}(2it\sqrt{1-n/L} + \varphi) \right|^2$ of (4.31). In ensemble average, the oscillations in the slope between different realization are cancelled with each other due to the phase fluctuation and end up with a moving average. The moving average of the slope behaves like the ramp down behavior in the numerical average.

D Constant Lanczos coefficients

To study the typical feature of Krylov complexity, we start with a special case in which the Lanczos coefficients are constant, namely,

$$a_n = 0, \quad b_n = 1, \quad (\text{D.1})$$

except $b_0 = b_L = 0$. Without loss of generality, we work at dimensionless quantities, so that spectrum $\{E_p\}$, Lanczos coefficients $\{a_n, b_n\}$, and time $\tau = \beta + it$ are dimensionless.

The $b_{n+1}^2 - b_n^2$ and $a_{n+1} - a_n$ terms in the Ehrenfest theorem (2.22) vanish except $b_1^2 - b_0^2 = 1$ and $b_L^2 - b_{L-1}^2 = -1$. So the growth of Krylov complexity are driven by the possibility on the two edges, namely,

$$\partial_t^2 K(t; \beta) = 2 \frac{|\phi_0(\beta + it)|^2 - |\phi_{L-1}(\beta + it)|^2}{S(2\beta)}. \quad (\text{D.2})$$

Eq. (D.1) effectively describe the flat Lanczos coefficients in a chaos system at the $n \ll L$ limit. Since the wave function is initially localized at $n = 0$, the short time evolution of the wave function as well as the Krylov complexity in a general system is effectively described by the first term of Eq. (D.2).

D.1 Eigenstate

From (2.8), we find that the orthogonal and normalized polynomial is given by the Chebyshev polynomial of second kind [67, 104]

$$\psi_n(E) = U_n(E/2). \quad (\text{D.3})$$

The eigenenergy and the measure are

$$E_p = 2 \cos \frac{\pi(L-p)}{L+1}, \quad |\langle E_p | 0 \rangle|^2 = \frac{4 - E_p^2}{2(L+1)}, \quad p = 0, 1, 2, \dots, L-1. \quad (\text{D.4})$$

At low temperature, according to (2.24), the complexity will converge to

$$K_{\text{low}}(\beta) \approx \frac{L-1}{2}, \quad (\text{D.5})$$

where the tedious sub-leading term is not shown. It describes the $\beta \gg L$ limit.

At the long-time average, according to (2.27), the plateau value of the complexity is given by

$$K_{\infty}(\beta) = \frac{L-1}{2}. \quad (\text{D.6})$$

D.2 Large dimension limit

In the large L limit, we can calculate the evolution of wave function and complexity analytically. The density of state and the measure are approximately

$$\rho(E) \approx \frac{L}{\pi\sqrt{4-E^2}}, \quad |\langle E|0\rangle|^2 \approx \frac{4-E^2}{2L}. \quad (\text{D.7})$$

The wave function is given by the integral

$$\phi_n(\tau) \approx \frac{1}{2\pi} \int_{-2}^2 \psi_n(E) e^{-\tau E} \sqrt{4-E^2} dE = (-1)^n \frac{n+1}{\tau} I_{n+1}(2\tau), \quad (\text{D.8})$$

where I_n is the n -th modified Bessel function of the first kind. $\phi_n(\tau)$ becomes nonzero for all n in this large L limit. We can calculate the survival amplitude and Krylov complexity along imaginary time

$$S(2\beta) \approx \frac{I_1(4\beta)}{2\beta}, \quad (\text{D.9})$$

$$K(0; \beta) \approx \frac{2\beta (I_0(2\beta)^2 + I_1(2\beta)^2)}{I_1(4\beta)} - 1 \approx 2\sqrt{\frac{2\beta}{\pi}} - 1, \quad \text{when } \beta \gg 1, \quad (\text{D.10})$$

where we have used the recursion relations $2nI_n(x) = x(I_{n-1}(x) - I_{n+1}(x))$ and $2I'_n(x) = I_{n-1}(x) + I_{n+1}(x)$. Along the real time, we use (D.2) and find

$$\partial_t^2 K(t; \beta) \approx 2 \frac{2\beta}{\beta^2 + t^2} \frac{|I_1(2\beta + i2t)|^2}{I_1(4\beta)}. \quad (\text{D.11})$$

We integrate over the real time and obtain the complexity different $\Delta K(t; \beta)$

$$\Delta K(t; \beta) \approx \begin{cases} {}_1F_2(-1/2; 1, 2; -4t^2) - 1 \approx \frac{16}{3\pi}t, & \beta = 0 \\ \sqrt{\frac{8}{\pi\beta}} (\sqrt{\beta^2 + t^2} - \beta) \approx \sqrt{\frac{8}{\pi\beta}}t, & \beta \gg 1 \end{cases}, \quad (\text{D.12})$$

where F is the generalized hypergeometric function and we show the linear growth at the last step. The above results show the typical square-to-linear-to-plateau growth of Krylov complexity along the real time at finite temperature. We compare these formulas to the numeric results in Fig. 19.

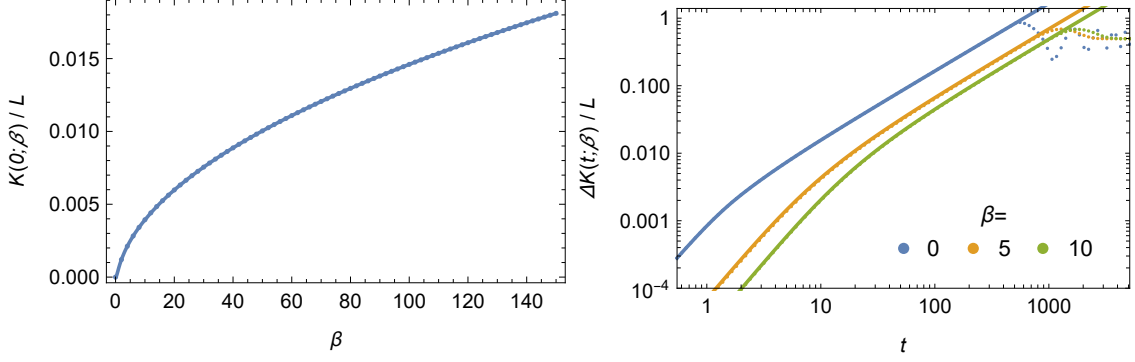


Figure 19. The Krylov complexity as a function of inverse temperature (left) and time (right) in the case of constant Lanczos coefficient with $L = 1024$. The dots represent the numerical results and the solid curves represent analytical approximation in (D.10) and (D.12).

D.3 Finite dimension effects

We would like to study the behavior of the Krylov complexity near the plateau time. We will consider a large but finite L , such that $\beta, t > L$ is accessible. For simplicity, we will adopt the continuous Schrödinger equation (A.4) with potential $\tilde{V}(y) = -2\Theta(y)\Theta(L - y)$ and the boundary conditions $\Phi(0) = \Phi(L) = 0$. The eigensystem are

$$E_k = \left(\frac{k\pi}{L}\right)^2 - 2, \quad \Phi_k(y) = \sqrt{\frac{2}{L}} \sin \frac{\pi ky}{L}, \quad k = 1, 2, \dots, \tilde{L} \quad (\text{D.13})$$

where k is originally bounded by the dimension of the Krylov space L , but we have released this constraint by consider the bound \tilde{L} instead and will sent $\tilde{L} \rightarrow \infty$ finally for simplicity. We consider the initial state $\tilde{\varphi}(\tau = 0) = \delta(y - \epsilon)$ locating beside the boundary with small distance ϵ . Its overlap to the eigenstate is $\langle E_k | \tilde{\varphi}(0) \rangle = \sqrt{2}\pi k\epsilon/L^{3/2}$. So the state evolves as

$$\tilde{\varphi}(\tau) = \frac{2\pi\epsilon^2}{L^2} \sum_{k=1}^{\tilde{L}} k e^{-E_k\tau} \sin \frac{\pi ky}{L}, \quad (\text{D.14})$$

Since the Lanczos coefficients are flat, the Krylov complexity K is the expectation value of the position operator y . The complexity operator on the energy basis are

$$K_{kl} = \langle E_k | y | E_l \rangle = \begin{cases} \frac{L}{2}, & k = l, \\ -\frac{8Lkl}{\pi^2(k^2 - l^2)^2}, & \text{odd } k + l. \\ 0, & \text{others} \end{cases} \quad (\text{D.15})$$

Its expectation value is

$$\begin{aligned}
\langle K \rangle &= \frac{\sum_{kl} \langle \tilde{\varphi}(\tau) | E_k \rangle K_{kl} \langle E_l | \tilde{\varphi}(\tau) \rangle}{\langle \tilde{\varphi}(\tau) | \tilde{\varphi}(\tau) \rangle} \\
&= \frac{L}{2} - \frac{\epsilon^2}{L^2 S(2\beta)} \\
&\quad \times \sum_{kl; \text{odd } k_+} \left(\frac{k_-}{k_+} - \frac{k_+}{k_-} \right)^2 \exp \left\{ -\frac{\pi^2}{2L^2} \left[\beta \left(k_-^2 + k_+^2 - \frac{8L^2}{\pi^2} \right) + 2ik_-k_+t \right] \right\},
\end{aligned} \tag{D.16}$$

where $\tau = \beta + it$, $k_{\pm} = k \pm l$, and

$$\begin{aligned}
S(2\beta) &= \langle \tilde{\varphi}(\beta) | \tilde{\varphi}(\beta) \rangle = \frac{2\pi^2 \epsilon^2}{L^3} \sum_k k^2 e^{\beta(4 - \frac{2\pi^2 k^2}{L^2})} \\
&\approx \frac{e^{4\beta} \epsilon^2}{8\beta^{3/2}} \left(\sqrt{\frac{2}{\pi}} \operatorname{erf} \left(\pi \sqrt{2\beta} \right) - 4e^{-2\pi^2 \beta} \sqrt{\beta} \right).
\end{aligned} \tag{D.17}$$

By taking the summation, one can get the value of Krylov complexity for general β and t .

References

- [1] V. Balasubramanian, P. Caputa, J.M. Magan and Q. Wu, *Quantum chaos and the complexity of spread of states*, *Phys. Rev. D* **106** (2022) 046007 [2202.06957].
- [2] F.J. Dyson, *Statistical theory of the energy levels of complex systems. i*, *Journal of Mathematical Physics* **3** (1962) 140.
- [3] T. Guhr, A. Muller-Groeling and H.A. Weidenmuller, *Random matrix theories in quantum physics: Common concepts*, *Phys. Rept.* **299** (1998) 189 [[cond-mat/9707301](#)].
- [4] O. Bohigas, M.J. Giannoni and C. Schmit, *Characterization of chaotic quantum spectra and universality of level fluctuation laws*, *Phys. Rev. Lett.* **52** (1984) 1.
- [5] F.J. Dyson, *A class of matrix ensembles*, *Journal of Mathematical Physics* **13** (1972) 90.
- [6] I. Dumitriu and A. Edelman, *Matrix models for beta ensembles*, *Journal of Mathematical Physics* **43** (2002) 5830.
- [7] A. Kitaev, “A simple model of quantum holography.” <http://online.kitp.ucsb.edu/online/entangled15/kitaev/> <http://online.kitp.ucsb.edu/online/entangled15/kitaev2/>, 2015.
- [8] J. Maldacena and D. Stanford, *Remarks on the sachdev-ye-kitaev model*, *Phys. Rev. D* **94** (2016) 106002 [1604.07818].

- [9] Y.-Z. You, A.W. Ludwig and C. Xu, *Sachdev-ye-kitaev model and thermalization on the boundary of many-body localized fermionic symmetry-protected topological states*, *Physical Review B* **95** (2017) 115150.
- [10] A.M. García-García and J.J.M. Verbaarschot, *Spectral and thermodynamic properties of the sachdev-ye-kitaev model*, *Phys. Rev. D* **94** (2016) 126010 [[1610.03816](#)].
- [11] P. Saad, S.H. Shenker and D. Stanford, *It gravity as a matrix integral*, [1903.11115](#).
- [12] E. Brézin and S. Hikami, *Spectral form factor in a random matrix theory*, *Physical Review E* **55** (1997) 4067.
- [13] R. Prange, *The spectral form factor is not self-averaging*, *Physical review letters* **78** (1997) 2280.
- [14] J.S. Cotler, G. Gur-Ari, M. Hanada, J. Polchinski, P. Saad, S.H. Shenker et al., *Black holes and random matrices*, *JHEP* **05** (2017) 118 [[1611.04650](#)].
- [15] J. Cotler, N. Hunter-Jones, J. Liu and B. Yoshida, *Chaos, complexity, and random matrices*, *JHEP* **11** (2017) 048 [[1706.05400](#)].
- [16] J. Liu, *Spectral form factors and late time quantum chaos*, *Phys. Rev. D* **98** (2018) 086026 [[1806.05316](#)].
- [17] S. Lloyd, *Ultimate physical limits to computation*, *Nature* **406** (2000) 1047 [[quant-ph/9908043](#)].
- [18] L. Susskind, *Computational complexity and black hole horizons*, *Fortsch. Phys.* **64** (2016) 24 [[1403.5695](#)].
- [19] D. Harlow et al., *Tf1 snowmass report: Quantum gravity, string theory, and black holes*, [2210.01737](#).
- [20] T. Faulkner, T. Hartman, M. Headrick, M. Rangamani and B. Swingle, *Snowmass white paper: Quantum information in quantum field theory and quantum gravity*, in *2022 Snowmass Summer Study*, 3, 2022 [[2203.07117](#)].
- [21] M.A. Nielsen, *A geometric approach to quantum circuit lower bounds*, *Quantum Info. Comput.* **6** (2006) 213–262 [[quant-ph/0502070](#)].
- [22] M.A. Nielsen, M.R. Dowling, M. Gu and A.C. Doherty, *Quantum computation as geometry*, *Science* **311** (2006) 1133 [[quant-ph/0603161](#)].
- [23] M.R. Dowling and M.A. Nielsen, *The geometry of quantum computation*, *Quantum Info. Comput.* **8** (2008) 861–899 [[quant-ph/0701004](#)].
- [24] S. Aaronson, *The complexity of quantum states and transformations: From quantum money to black holes*, [1607.05256](#).
- [25] J. Watrous, *Quantum computational complexity*, in *Encyclopedia of Complexity and Systems Science*, 2008 [[0804.3401](#)].
- [26] R. Jefferson and R.C. Myers, *Circuit complexity in quantum field theory*, *JHEP* **10** (2017) 107 [[1707.08570](#)].

- [27] S. Chapman, M.P. Heller, H. Marrochio and F. Pastawski, *Toward a definition of complexity for quantum field theory states*, *Phys. Rev. Lett.* **120** (2018) 121602 [[1707.08582](#)].
- [28] L. Hackl and R.C. Myers, *Circuit complexity for free fermions*, *JHEP* **07** (2018) 139 [[1803.10638](#)].
- [29] J. Molina-Vilaplana and A. Del Campo, *Complexity functionals and complexity growth limits in continuous mera circuits*, *JHEP* **08** (2018) 012 [[1803.02356](#)].
- [30] R. Khan, C. Krishnan and S. Sharma, *Circuit complexity in fermionic field theory*, *Phys. Rev. D* **98** (2018) 126001 [[1801.07620](#)].
- [31] V. Balasubramanian, M. Decross, A. Kar and O. Parrikar, *Quantum complexity of time evolution with chaotic hamiltonians*, *JHEP* **01** (2020) 134 [[1905.05765](#)].
- [32] T. Ali, A. Bhattacharyya, S.S. Haque, E.H. Kim, N. Moynihan and J. Murugan, *Chaos and complexity in quantum mechanics*, *Phys. Rev. D* **101** (2020) 026021 [[1905.13534](#)].
- [33] A. Bhattacharyya, S.S. Haque and E.H. Kim, *Complexity from the reduced density matrix: a new diagnostic for chaos*, *JHEP* **10** (2021) 028 [[2011.04705](#)].
- [34] A. Bhattacharyya, W. Chemissany, S. Shajidul Haque and B. Yan, *Towards the web of quantum chaos diagnostics*, *Eur. Phys. J. C* **82** (2022) 87 [[1909.01894](#)].
- [35] J.M. Magán, *Black holes, complexity and quantum chaos*, *JHEP* **09** (2018) 043 [[1805.05839](#)].
- [36] P. Caputa and J.M. Magan, *Quantum computation as gravity*, *Phys. Rev. Lett.* **122** (2019) 231302 [[1807.04422](#)].
- [37] J. Erdmenger, M. Gerbershagen and A.-L. Weigel, *Complexity measures from geometric actions on virasoro and kac-moody orbits*, *JHEP* **11** (2020) 003 [[2004.03619](#)].
- [38] P. Basteiro, J. Erdmenger, P. Fries, F. Goth, I. Matthaiakakis and R. Meyer, *Quantum complexity as hydrodynamics*, *Phys. Rev. D* **106** (2022) 065016 [[2109.01152](#)].
- [39] C. Ly, R. Zhang and Q. Zhou, *Building krylov complexity from circuit complexity*, [2303.07343](#).
- [40] D.A. Roberts and B. Yoshida, *Chaos and complexity by design*, *JHEP* **04** (2017) 121 [[1610.04903](#)].
- [41] J.M. Maldacena, *The large n limit of superconformal field theories and supergravity*, *Adv. Theor. Math. Phys.* **2** (1998) 231 [[hep-th/9711200](#)].
- [42] L. Susskind and Y. Zhao, *Switchbacks and the bridge to nowhere*, [1408.2823](#).
- [43] D. Stanford and L. Susskind, *Complexity and shock wave geometries*, *Phys. Rev. D* **90** (2014) 126007 [[1406.2678](#)].

- [44] A.R. Brown, D.A. Roberts, L. Susskind, B. Swingle and Y. Zhao, *Complexity, action, and black holes*, *Phys. Rev. D* **93** (2016) 086006 [[1512.04993](#)].
- [45] L. Susskind, *Complexity and Newton's Laws*, *Front. in Phys.* **8** (2020) 262 [[1904.12819](#)].
- [46] L. Susskind and Y. Zhao, *Complexity and Momentum*, *JHEP* **03** (2021) 239 [[2006.03019](#)].
- [47] A.R. Brown and L. Susskind, *Second law of quantum complexity*, *Phys. Rev. D* **97** (2018) 086015 [[1701.01107](#)].
- [48] J.M. Maldacena, *Eternal black holes in anti-de sitter*, *JHEP* **04** (2003) 021 [[hep-th/0106112](#)].
- [49] R. Abt, J. Erdmenger, H. Hinrichsen, C.M. Melby-Thompson, R. Meyer, C. Northe et al., *Topological complexity in ads_3/cft_2* , *Fortsch. Phys.* **66** (2018) 1800034 [[1710.01327](#)].
- [50] S. Chapman, J. Eisert, L. Hackl, M.P. Heller, R. Jefferson, H. Marrochio et al., *Complexity and entanglement for thermofield double states*, *SciPost Phys.* **6** (2019) 034 [[1810.05151](#)].
- [51] A.R. Brown, H. Gharibyan, A. Streicher, L. Susskind, L. Thorlacius and Y. Zhao, *Falling toward charged black holes*, *Phys. Rev. D* **98** (2018) 126016 [[1804.04156](#)].
- [52] L. Susskind, *Why do things fall?*, [1802.01198](#).
- [53] H.W. Lin and L. Susskind, *Complexity geometry and schwarzian dynamics*, *JHEP* **01** (2020) 087 [[1911.02603](#)].
- [54] A.R. Brown, H. Gharibyan, H.W. Lin, L. Susskind, L. Thorlacius and Y. Zhao, *Complexity of jackiw-teitelboim gravity*, *Phys. Rev. D* **99** (2019) 046016 [[1810.08741](#)].
- [55] M. Flory and M.P. Heller, *Geometry of complexity in conformal field theory*, *Phys. Rev. Res.* **2** (2020) 043438 [[2005.02415](#)].
- [56] M. Flory and M.P. Heller, *Conformal field theory complexity from euler-arnold equations*, *JHEP* **12** (2020) 091 [[2007.11555](#)].
- [57] N. Chagnet, S. Chapman, J. de Boer and C. Zukowski, *Complexity for conformal field theories in general dimensions*, *Phys. Rev. Lett.* **128** (2022) 051601 [[2103.06920](#)].
- [58] J. Erdmenger, M. Flory, M. Gerbershagen, M.P. Heller and A.-L. Weigel, *Exact gravity duals for simple quantum circuits*, *SciPost Phys.* **13** (2022) 061 [[2112.12158](#)].
- [59] J. Erdmenger, M. Gerbershagen, M.P. Heller and A.-L. Weigel, *From complexity geometry to holographic spacetime*, [2212.00043](#).
- [60] D.E. Parker, X. Cao, A. Avdoshkin, T. Scaffidi and E. Altman, *A universal operator growth hypothesis*, *Phys. Rev. X* **9** (2019) 041017 [[1812.08657](#)].

- [61] J. Barbón, E. Rabinovici, R. Shir and R. Sinha, *On the evolution of operator complexity beyond scrambling*, *JHEP* **10** (2019) 264 [[1907.05393](#)].
- [62] E. Rabinovici, A. Sánchez-Garrido, R. Shir and J. Sonner, *Operator complexity: a journey to the edge of krylov space*, [2009.01862](#).
- [63] S.-K. Jian, B. Swingle and Z.-Y. Xian, *Complexity growth of operators in the syk model and in jt gravity*, *JHEP* **03** (2021) 014 [[2008.12274](#)].
- [64] A. Dymarsky and M. Smolkin, *Krylov complexity in conformal field theory*, *Phys. Rev. D* **104** (2021) L081702 [[2104.09514](#)].
- [65] P. Caputa, J.M. Magan and D. Patramanis, *Geometry of krylov complexity*, *Phys. Rev. Res.* **4** (2022) 013041 [[2109.03824](#)].
- [66] V. Balasubramanian, J.M. Magan and Q. Wu, *A tale of two hungarians: Tridiagonalizing random matrices*, [2208.08452](#).
- [67] A. Dymarsky and A. Gorsky, *Quantum chaos as delocalization in krylov space*, *Phys. Rev. B* **102** (2020) 085137 [[1912.12227](#)].
- [68] A. Avdoshkin and A. Dymarsky, *Euclidean operator growth and quantum chaos*, *Phys. Rev. Res.* **2** (2020) 043234 [[1911.09672](#)].
- [69] V. Viswanath and G. Müller, *The recursion method: application to many-body dynamics*, vol. 23, Springer Science & Business Media (2008).
- [70] C. Lanczos, *An iteration method for the solution of the eigenvalue problem of linear differential and integral operators*, *Journal of research of the National Bureau of Standards* **45** (1950) 255.
- [71] I. Gelfand and M. Neumark, *On the imbedding of normed rings into the ring of operators in hilbert space*, *Contemporary Mathematics* **167** (1994) 3.
- [72] I.E. Segal, *Irreducible representations of operator algebras*, *Bulletin of the American Mathematical Society* **53** (1947) 73.
- [73] J.M. Magán and J. Simón, *On operator growth and emergent poincaré symmetries*, *JHEP* **05** (2020) 071 [[2002.03865](#)].
- [74] S.S. Haque, J. Murugan, M. Tladi and H.J.R. Van Zyl, *Krylov complexity for jacobi coherent states*, [2212.13758](#).
- [75] B. Bhattacharjee, S. Sur and P. Nandy, *Probing quantum scars and weak ergodicity breaking through quantum complexity*, *Phys. Rev. B* **106** (2022) 205150 [[2208.05503](#)].
- [76] J.L.F. Barbón, E. Rabinovici, R. Shir and R. Sinha, *On the evolution of operator complexity beyond scrambling*, *JHEP* **10** (2019) 264 [[1907.05393](#)].
- [77] D.A. Roberts, D. Stanford and A. Streicher, *Operator growth in the syk model*, *JHEP* **06** (2018) 122 [[1802.02633](#)].
- [78] X.-L. Qi and A. Streicher, *Quantum epidemiology: Operator growth, thermal effects, and syk*, *JHEP* **08** (2019) 012 [[1810.11958](#)].

- [79] S.H. Shenker and D. Stanford, *Black holes and the butterfly effect*, *JHEP* **03** (2014) 067 [[1306.0622](#)].
- [80] D.A. Roberts, D. Stanford and L. Susskind, *Localized shocks*, *JHEP* **03** (2015) 051 [[1409.8180](#)].
- [81] T.G. Mertens, G.J. Turiaci and H.L. Verlinde, *Solving the schwarzian via the conformal bootstrap*, *JHEP* **08** (2017) 136 [[1705.08408](#)].
- [82] S.H. Shenker and D. Stanford, *Multiple shocks*, *JHEP* **12** (2014) 046 [[1312.3296](#)].
- [83] B. Bhattacharjee, X. Cao, P. Nandy and T. Pathak, *Krylov complexity in saddle-dominated scrambling*, *JHEP* **05** (2022) 174 [[2203.03534](#)].
- [84] B.L. Español and D.A. Wisniacki, *Assessing the saturation of krylov complexity as a measure of chaos*, *Phys. Rev. E* **107** (2023) 024217 [[2212.06619](#)].
- [85] A. Kar, L. Lamprou, M. Rozali and J. Sully, *Random matrix theory for complexity growth and black hole interiors*, *JHEP* **01** (2022) 016 [[2106.02046](#)].
- [86] E. Rabinovici, A. Sánchez-Garrido, R. Shir and J. Sonner, *Krylov localization and suppression of complexity*, *JHEP* **03** (2022) 211 [[2112.12128](#)].
- [87] E. Rabinovici, A. Sánchez-Garrido, R. Shir and J. Sonner, *Krylov complexity from integrability to chaos*, *JHEP* **07** (2022) 151 [[2207.07701](#)].
- [88] M. Alishahiha and S. Banerjee, *A universal approach to krylov state and operator complexities*, [2212.10583](#).
- [89] B. Bhattacharjee, P. Nandy and T. Pathak, *Krylov complexity in large- q and double-scaled syk model*, [2210.02474](#).
- [90] S. He, P.H.C. Lau, Z.-Y. Xian and L. Zhao, *Quantum chaos, scrambling and operator growth in $t\bar{T}$ deformed syk models*, *JHEP* **12** (2022) 070 [[2209.14936](#)].
- [91] P. Caputa and S. Datta, *Operator growth in 2d cft*, *JHEP* **12** (2021) 188 [[2110.10519](#)].
- [92] S. Khetrpal, *Chaos and operator growth in 2d cft*, *JHEP* **03** (2023) 176 [[2210.15860](#)].
- [93] A. Kundu, V. Malvimat and R. Sinha, *State dependence of krylov complexity in 2d cfts*, [2303.03426](#).
- [94] H.A. Camargo, V. Jahnke, K.-Y. Kim and M. Nishida, *Krylov complexity in free and interacting scalar field theories with bounded power spectrum*, [2212.14702](#).
- [95] A. Avdoshkin, A. Dymarsky and M. Smolkin, *Krylov complexity in quantum field theory, and beyond*, [2212.14429](#).
- [96] F.B. Trigueros and C.-J. Lin, *Krylov complexity of many-body localization: Operator localization in krylov basis*, *SciPost Phys.* **13** (2022) 037 [[2112.04722](#)].
- [97] C. Liu, H. Tang and H. Zhai, *Krylov complexity in open quantum systems*, [2207.13603](#).

- [98] A. Bhattacharya, P. Nandy, P.P. Nath and H. Sahu, *Operator growth and krylov construction in dissipative open quantum systems*, *JHEP* **12** (2022) 081 [[2207.05347](#)].
- [99] B. Bhattacharjee, X. Cao, P. Nandy and T. Pathak, *Operator growth in open quantum systems: lessons from the dissipative syk*, [2212.06180](#).
- [100] A. Bhattacharya, P. Nandy, P.P. Nath and H. Sahu, *On krylov complexity in open systems: an approach via bi-lanczos algorithm*, [2303.04175](#).
- [101] P. Caputa, N. Gupta, S.S. Haque, S. Liu, J. Murugan and H.J.R. Van Zyl, *Spread complexity and topological transitions in the kitaev chain*, *JHEP* **01** (2023) 120 [[2208.06311](#)].
- [102] P. Caputa and S. Liu, *Quantum complexity and topological phases of matter*, *Phys. Rev. B* **106** (2022) 195125 [[2205.05688](#)].
- [103] J. Kim, J. Murugan, J. Olle and D. Rosa, *Operator delocalization in quantum networks*, *Phys. Rev. A* **105** (2022) L010201 [[2109.05301](#)].
- [104] W. Mück and Y. Yang, *Krylov complexity and orthogonal polynomials*, [2205.12815](#).
- [105] A. Avdoshkin and A. Dymarsky, *Euclidean operator growth and quantum chaos*, [1911.09672](#).
- [106] L.V. Iliesiu, M. Mezei and G. Sárosi, *The volume of the black hole interior at late times*, *JHEP* **07** (2022) 073 [[2107.06286](#)].
- [107] E. Brézin and S. Hikami, *Spectral form factor in a random matrix theory*, *Phys. Rev. E* **55** (1997) 4067.
- [108] M. Winer, S.-K. Jian and B. Swingle, *An exponential ramp in the quadratic sachdev-ye-kitaev model*, *Phys. Rev. Lett.* **125** (2020) 250602 [[2006.15152](#)].
- [109] N. Hörnedal, N. Carabba, A.S. Matsoukas-Roubeas and A. del Campo, *Ultimate speed limits to the growth of operator complexity*, *Commun. Phys.* **5** (2022) 207 [[2202.05006](#)].
- [110] M. Berkooz, M. Isachenkov, V. Narovlansky and G. Torrents, *Towards a full solution of the large n double-scaled syk model*, *JHEP* **03** (2019) 079 [[1811.02584](#)].
- [111] M. Berkooz, P. Narayan and J. Simon, *Chord diagrams, exact correlators in spin glasses and black hole bulk reconstruction*, *JHEP* **08** (2018) 192 [[1806.04380](#)].
- [112] H.W. Lin, *The bulk hilbert space of double scaled syk*, *JHEP* **11** (2022) 060 [[2208.07032](#)].
- [113] A. Chattopadhyay, A. Mitra and H.J.R. van Zyl, *Spread complexity as classical dilaton solutions*, [2302.10489](#).